

Accepted Manuscript

Synthesis and biological evaluation of curcumin inspired imidazo[1,2-*a*]pyridine analogues as tubulin polymerization inhibitors

P.V.Sri Ramya, Lalita Guntuku, Srinivas Angapelly, Chander Singh Digwal, Uppu Jaya Lakshmi, Dilep Kumar Sigalapalli, Bathini Nagendra Babu, V.G.M. Naidu, Ahmed Kamal

PII: S0223-5234(17)30895-4

DOI: [10.1016/j.ejmech.2017.11.010](https://doi.org/10.1016/j.ejmech.2017.11.010)

Reference: EJMECH 9885

To appear in: *European Journal of Medicinal Chemistry*

Received Date: 4 October 2017

Revised Date: 3 November 2017

Accepted Date: 3 November 2017

Please cite this article as: P.V.S. Ramya, L. Guntuku, S. Angapelly, C.S. Digwal, U.J. Lakshmi, D.K. Sigalapalli, B.N. Babu, V.G.M. Naidu, A. Kamal, Synthesis and biological evaluation of curcumin inspired imidazo[1,2-*a*]pyridine analogues as tubulin polymerization inhibitors, *European Journal of Medicinal Chemistry* (2017), doi: 10.1016/j.ejmech.2017.11.010.

This is a PDF file of an unedited manuscript that has been accepted for publication. As a service to our customers we are providing this early version of the manuscript. The manuscript will undergo copyediting, typesetting, and review of the resulting proof before it is published in its final form. Please note that during the production process errors may be discovered which could affect the content, and all legal disclaimers that apply to the journal pertain.



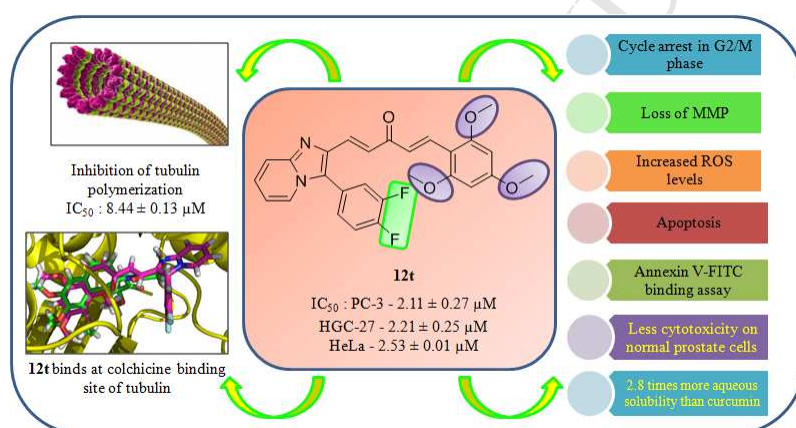
Graphical Abstract

Synthesis and biological evaluation of curcumin inspired imidazo[1,2-*a*]pyridine analogues as tubulin polymerization inhibitors

P. V. Sri Ramya,^a Lalita Guntuku,^b Srinivas Angapelly,^a Chander Singh Digwal,^a Uppu Jaya Lakshmi,^b Dilep Kumar Sigalapalli,^a Bathini Nagendra Babu,^a V.G.M. Naidu,^b Ahmed Kamal^{a*}

^aDepartment of Medicinal Chemistry, National Institute of Pharmaceutical Education and Research (NIPER), Hyderabad 500037, India.

^bDepartment of Pharmacology and Toxicology, National Institute of Pharmaceutical Education and Research (NIPER), Hyderabad 500037, India.



Synthesis and biological evaluation of curcumin inspired imidazo[1,2-*a*]pyridine analogues as tubulin polymerization inhibitors

P. V. Sri Ramya,^a Lalita Guntuku,^b Srinivas Angapelly,^a Chander Singh Digwal,^a Uppu Jaya Lakshmi,^b Dilep Kumar Sigalapalli,^a Bathini Nagendra Babu,^a V.G.M. Naidu,^b Ahmed Kamal^{a*}

^a*Department of Medicinal Chemistry, National Institute of Pharmaceutical Education and Research (NIPER), Hyderabad 500037, India.*

^b*Department of Pharmacology and Toxicology, National Institute of Pharmaceutical Education and Research (NIPER), Hyderabad 500037, India.*

Abstract

With an aim to develop new curcumin inspired analogues as potent anticancer agents, we synthesized a series of (1*E*,4*E*)-1-phenyl-5-(3-phenylimidazo[1,2-*a*]pyridin-2-yl)penta-1,4-dien-3-ones (**12a–t**) as tubulin polymerization inhibitors. An initial screening was carried out to evaluate their cytotoxic potential on a panel of six cancer cell lines namely, cervical (HeLa), gastric (HGC-27), lung (NCI-H460), prostate (DU-145 and PC-3) and breast (4T1), using MTT assay. Among the compounds tested, compounds **12e**, **12r** and **12t** showed potent growth inhibition and **12t** {(1*E*,4*E*)-1-(3-(3,4-difluorophenyl)imidazo[1,2-*a*]pyridin-2-yl)-5-(2,4,6-trimethoxyphenyl)penta-1,4-dien-3-one} being the most active member of the series inhibited the growth of all the tested cell lines with IC₅₀ values varying from 1.7 – 2.97 μM. Moreover, **12t** showed promising cytotoxicity on PC-3, HGC-27 and HeLa cell lines with IC₅₀ values of 2.11 ± 0.27 μM, 2.21 ± 0.25 μM and 2.53 ± 0.01 μM respectively. The results from aqueous solubility test showed that compounds **12e** and **12t** have 1.7 and 2.8 times more aqueous solubility than curcumin. Interestingly, the most active compound **12t** was found to be nearly 2 times more selective on PC-3 cells as well as safe on normal human prostate (RWPE-1) cells. In addition, compound **12t** efficiently inhibited tubulin polymerization with IC₅₀ value of 8.44 ± 0.13 μM and molecular modelling studies disclosed that **12t** binds at the colchicine binding site of the tubulin. Cell cycle analysis revealed that **12t** arrests PC-3 cells in G2/M phase in a dose dependant manner. Further, treatment of PC-3 cells with **12t** showed typical apoptotic morphology, also led to the impairment of mitochondrial membrane potential (ΔΨ_m) and increased levels of reactive oxygen species (ROS). Altogether, the results from acridine

orange/ethidium bromide (AO-EB) and DAPI staining studies, annexin V-FITC/propidium iodide staining assay, analysis of mitochondrial membrane potential ($D\Psi_m$) and reactive oxygen species (ROS) levels undoubtedly demonstrated the induction of apoptosis in PC-3 cells by compound **12t**.

Keywords: Curcumin inspired analogues, imidazo[1,2-*a*]pyridine, cytotoxic, apoptosis, Claisen-Schmidt condensation.

*Corresponding author: Tel.: +91 40 27193157; fax: +91 40 27193189. *E-mail:* ahmedkamal@iict.res.in

1. Introduction

Natural products have traditionally been a magnificent source of novel medicinal leads, and their contribution in drug discovery is uniquely pronounced in the domain of cancer pharmacology, where the fraction of the drugs derived from natural products amounts to 60% [1]. Curcumin (1,7-bis(4-hydroxy 3-methoxy phenyl)-1,6-heptadione-3,5-dione or diferuloylmethane) (**Figure 1, 1**) is one of such natural products, obtained from the rhizomes of the plant Turmeric (*Curcuma longa*) [2]. Curcumin was found to be a highly pleiotropic molecule that interacts with a diverse variety of molecular targets and impede with multiple cell signaling pathways, including proliferation (HER-2, AP-1 and EGFR), angiogenesis (VEGF), apoptosis (activation of caspases and down regulation of antiapoptotic gene products), and inflammation (NF- κ B, TNF, IL-1, IL-6, COX-2, and 5-LOX) [3-12]. Therefore it possess a diverse range of biological activities such as anti-carcinogenic [13], antioxidant [14], antitumor [15], anti-angiogenesis [16], anti-inflammatory [17], antithrombotic [18], antihepatotoxic [19], hypoglycemic [20] and antihyperlipidaemic [21]. Additionally, numerous studies have shown that curcumin has beneficial effects in the treatment of myocardial infarction, Alzheimer's disease, rheumatoid arthritis, human immunodeficiency virus (HIV) syndrome and psoriasis [22]. Further, curcumin is non-toxic even at high dosages and has been categorized as 'generally recognized as safe' (GRAS) by the National Cancer Institute [23,24]. These multiple biological properties attracted clinicians to investigate the therapeutic potential of curcumin and nearly 65 clinical trials are being carried out worldwide in order to accelerate this lead molecule from kitchen to clinic [21,25,26]. Despite of the broad spectrum activities and safety profile, it is not yet approved as a

therapeutic agent because of its poor oral bioavailability, poor water and plasma solubility as noticeable from the data of pharmacokinetic and pharmacodynamics studies [23,24]. Hence, there have been significant efforts to synthesize analogues of curcumin with a similar safety profile, besides increased activity and improved oral bioavailability and the process is quite on the way of progress, with a huge number of successes.

Curcumin has substantially been used as a lead compound to design and synthesize analogs with improved activity. The reported studies focused mainly on modifications in the β -diketone structure and aryl substitution pattern of curcumin. As evident from the reported studies, the β -diketone moiety of curcumin seems to be a specific substrate of a series of aldo-keto reductases and can be metabolised rapidly *in vivo* [27,28] whereas monoketone analogs generally have improved pharmacokinetic profiles over curcumin. Moreover, monoketone analogues (**Figure 1**, curcumin analogues **2-7**) containing 5/6 membered heterocycles such as quinazoline [29], thiazole [30], imidazole [31], chromone [32] and indole [33] moieties have been well studied in the literature for their improved cytotoxic potency than curcumin. Thus, the 1,5-diaryl/diheteroaryl/arylheteroaryl penta-1,4-dien-3-one moiety portrayed by these compounds, can be considered as an optimal scaffold for developing novel curcumin mimics/analogues as potent anticancer agents. It is hence worthwhile to instigate extensive investigation of this category of curcumin analogues as potential cytotoxic agents.

<Insert Figure 1 here>

On the contrary, imidazopyridine is one of the important fused bicyclic 5-6 heterocycles, with a wide range of biological activities such as antitumor, anti-apoptotic, hypnoselective, antibacterial, antifungal, antiviral, antiprotozoal and anti-inflammatory. Furthermore, imidazo[1,2-*a*]pyridine is regarded as a “drug prejudice” moiety because of its unavoidable occurrence in numerous clinical drugs that includes zolpidem, saripidem, olprinone, zolimidine, rifaximin and drug candidates such as ND-09759 and Q203, which are at present in pre-clinical and phase I clinical development respectively for tuberculosis (**Figure 2**) [34,35]. In recent years, imidazopyridine/pyrimidine chalcones [36], 2-phenyl-imidazo[1,2-*a*]pyridine analogues (tubulin polymerization inhibitors) [37], sulfonylhydrazone-substituted imidazo[1,2-*a*]pyridines (PI3 kinase p110 α inhibitors) [38] and the other imidazo-[1,2-*a*]pyridine derivatives acting on

Nek2 [39] and c-Met kinases [40] (**Figure 2**) have been extensively studied in the literature for their excellent antitumor activity.

<Insert Figure 2 here>

Inspired by the synthetic feasibility and biological activities of imidazo[1,2-*a*]pyridine derivatives, it would thus be considering beneficial to synthesize curcumin inspired imidazo[1,2-*a*]pyridine analogues, possessing a five-carbon dienone linear linker attached to substituted imidazo[1,2-*a*]pyridine and phenyl motifs on either sides of it and evaluate their anticancer activity (**Figure 3**). In line with our interest in the development of novel curcumin inspired analogues [33,41], herein we wish to report curcumin inspired imidazo[1,2-*a*]pyridine derivatives as tubulin polymerization inhibitors.

<Insert Figure 3 here>

2. Results and discussion

2.1. Chemistry

The target compounds (1*E*,4*E*)-1-phenyl-5-(3-phenylimidazo[1,2-*a*]pyridin-2-yl)penta-1,4-dien-3-ones (**12a–t**) were synthesized by employing Claisen-Schmidt condensation between (i) 3-substituted imidazo[1,2-*a*]pyridine-2-carbaldehyde (**11**), and (ii) a substituted chalcone (**3**) as depicted in **Scheme 1**. Initially, chalcones (**3**) were prepared by NaOH-catalysed Claisen-Schmidt condensation of appropriately substituted benzaldehydes (**1**) with acetone [42] (a, **Scheme 1**). The next core structural element, aldehyde (**11**) (b, **Scheme 1**) was synthesized by following a 5-step scheme, starting from 2-amino pyridine and ethylbromopyruvate to afford ester intermediate (**6**) [43]. Later, it was iodinated with *N*-iodosuccinimide [44] to form intermediate **7** and in the next step, it underwent Suzuki coupling with different phenyl boronic acids in the presence of Pd(PPh₃)₄/Na₂CO₃ [45] to give intermediate **9**. Further, it was reduced to the corresponding alcohol (**10**) by using LiAlH₄ [43] and then oxidized to the respective aldehyde (**11**) in the presence of Dess-Martin periodinane [46]. Finally, CH₃ONa-catalysed Claisen-Schmidt condensation of chalcone (**3**) and aldehyde (**11**) furnished the target compounds **12a–t** in moderate to very good yields (c, **Scheme 1**) [47].

<Insert Scheme 1 here>

All the synthesized compounds (**12a–t**) were unambiguously characterized by using FT-IR, HRMS, ^1H and ^{13}C NMR spectroscopy. The ^1H NMR spectrum of **12a** showed a sharp singlet of methoxy protons at δ 3.85 and rest all protons appeared in the range of δ 8.10 – 6.78. In the ^{13}C NMR spectrum of **12a**, the carbonyl and methoxy carbons appeared at δ 189.0 and 55.4 respectively and the remaining carbons appeared in the range of δ 161.5 – 112.8. Nearly similar patterns were noticed in ^1H and ^{13}C NMR spectra of all the compounds (**12a–t**). The FT-IR spectrum of **12a** showed a sharp band at 1651.8 cm^{-1} which confirmed the presence of ketone functionality. The HRMS (ESI) of **12a–t** showed characteristic $[\text{M}+\text{H}]^+$ corresponding peaks equivalent to their molecular formulae.

2.2. Biological evaluation

2.2.1. *In vitro* anticancer activity

The newly synthesized curcumin inspired imidazo[1,2-*a*]pyridine analogues (**12a–t**) were screened for their *in vitro* cytotoxicity against selected cancer cell lines viz. cervical (HeLa), gastric (HGC-27), lung (NCI-H460), prostate (DU-145 and PC-3), breast (4T1) and one normal human prostate epithelial cell (RWPE-1) using 3-(4,5-dimethylthiazol-2-yl)-2,5-diphenyltetrazolium bromide (MTT) assay [48]. The IC_{50} (μM) values (concentration required to cause 50% inhibition of the viability of cancer cells) of test compounds **12a–t** and the standard, curcumin and vincristine sulphate are shown in **Table 1**.

In order to understand the structure-activity relationship (SAR), we used diversified substitutions on the phenyl ring of the chalcone as well as the phenyl ring attached to the imidazo[1,2-*a*]pyridine moiety of these curcumin inspired analogues. From the preliminary results, it is evident that some of the synthesized compounds exhibited moderate to potent cytotoxicity against the tested cancer cell lines with IC_{50} values in the range of 1.67 ± 0.34 to 10.27 ± 0.25 μM . From the close analysis of **Table 1**, it can be observed that compounds **12c**, **12e**, **12n**, **12o**, **12q**, **12r**, **12s** and **12t** were the most active members of this series and the remaining compounds were almost inactive against the tested cell lines. Compounds **12a**, **12b**, **12d** and **12f** carrying 3-phenylimidazo[1,2-*a*]pyridine moiety and 4-methoxy/2,4-dimethoxy/3,4-dimethoxy/2,4,6-trimethoxy substitutions respectively on the phenyl ring of the chalcone were found to be inactive on the cell lines screened (IC_{50} values of $> 10\ \mu\text{M}$), whereas **12c** and **12e** possessing 2,5-

dimethoxy and 2,4,5-trimethoxy substitutions respectively exhibited potent cytotoxicity on nearly all the cell lines examined with IC_{50} values ranging from 1.67 – 7.08 μM . Surprisingly, compounds **12g**, **12h**, **12i** and **12j** which contain 3-(3-methoxy)phenylimidazo[1,2-*a*]pyridine moiety and 4-methoxy/2,4-dimethoxy/2,5-dimethoxy/3,4-dimethoxy substitutions respectively, did not show significant cytotoxicity at 10 μM . Similarly, compounds **12k**, **12l** and **12m** having 3-(4-methoxy)phenylimidazo[1,2-*a*]pyridine moiety and 4-methoxy/2,4-dimethoxy/2,5-dimethoxy substitutions respectively on the phenyl ring of the chalcone were found to be inactive. Interestingly, compounds **12n** and **12o** containing 3-(4-methoxy)phenylimidazo[1,2-*a*]pyridine moiety and 3,4-dimethoxy or 2,4,5-trimethoxy substitutions respectively on the phenyl ring of the chalcone displayed considerable cytotoxicity with IC_{50} values ranging from 3.64 – 9.41 μM . Compound **12p** with 3-(3,4-difluoro)phenylimidazo[1,2-*a*]pyridine moiety and 4-methoxy substitution on the chalcone showed IC_{50} of > 10 μM , while **12q** with 2,4-dimethoxy group on the chalcone showed cytotoxicity in the range of 8.41 – 10.27 μM . Importantly, **12r**, **12s** and **12t** holding 3-(3,4-difluoro)phenylimidazo[1,2-*a*]pyridine moiety and 2,5-dimethoxy/3,4-dimethoxy/2,4,6-trimethoxy substitutions respectively on the phenyl ring of the chalcone displayed potent cytotoxicity on all the cell lines screened with IC_{50} varying from 1.71 – 6.35 μM . Compound **12r** was active on all cell lines tested, especially PC-3 with IC_{50} of 2.84 ± 0.58 μM . Further, compound **12t**, the most active member of the series exhibited remarkable cytotoxicity on HeLa (2.53 ± 0.01 μM), HGC-27 (2.21 ± 0.25 μM), NCI-H460 (2.63 ± 0.05 μM), DU145 (2.97 ± 0.08 μM), PC-3 (2.11 ± 0.27 μM) and 4T1 (1.71 ± 0.11 μM) cell lines.

<Insert Table 1 here>

The impact of substitution on chalcones and imidazo[1,2-*a*]pyridine is interesting and the following conclusions have been drawn from the structure-activity relationship (SAR) analysis (**Figure 4**) of these compounds:

- a. From the IC_{50} values, in general, it can be noted that the presence of electron donating (3-methoxy or 4-methoxy) groups on the phenyl ring attached to imidazo[1,2-*a*]pyridine did not produce the bioactive compounds (**12g–m**) with the exception for compounds **12n** and **12o**.
- b. Compounds without any substitution on the phenyl ring linked to imidazo[1,2-*a*]pyridine and with mono or di or trimethoxy substitutions on the chalcone (**12a**, **12b**, **12d** and **12f**) were

nearly inactive at 10 μM , while compounds with 2,5-dimethoxy (**12c**) or 2,4,5-trimethoxy (**12e**) substitutions showed significant cytotoxicity.

c. In general, compounds with electron withdrawing (fluoro) groups on the phenyl ring attached to imidazo[1,2-*a*]pyridine (**12q–t**) were more potent, compound **12p** being the exceptional case, than compounds having unsubstituted phenyl or phenyl ring with electron donating groups (methoxy): the order may be electron withdrawing > neutral > electron donating.

d. Additionally, most of the compounds containing dimethoxy or trimethoxy group on the chalcone showed enhanced cytotoxicity than mono methoxy compounds.

<Insert Figure 4 here>

By comparing the IC_{50} values of compounds with that of curcumin, **12c**, **12e**, **12n–o**, **12q–t** were considered as more potent than curcumin (**Table 2**). They are 1.8 to 6.5 times, 3.9 to 11.1 times, and 2.1 to 8.9 times, respectively, more potent than curcumin on human lung cancer cell line (NCI-H460) and two human prostate cancer cell lines (DU145 and PC-3). Further, the most active compound **12t** is 6.5 times, 11.1 times and 8.9 times more cytotoxic on NCI-H460, DU-145 and PC-3 cell lines, respectively, than curcumin.

<Insert Table 2 here>

The aqueous solubility of the most active curcumin inspired analogues **12e** and **12t** was measured in comparison to curcumin by making their saturated aqueous solutions in milli-Q water [49]. The amount of compound solubilized was determined spectrophotometrically by scanning at 200 – 600 nm. **Figure 5** shows the UV-visible spectra recorded for compounds **12e** and **12t**. The results demonstrate that **12e** and **12t** have 1.7 and 2.8 times more aqueous solubility than curcumin.

<Insert Figure 5 here>

To find out the selectivity towards cancer cells, the most active compound **12t** was tested on normal human prostate epithelial cell line (RWPE-1). Interestingly, compound **12t** was found to be almost 2 times more selective for PC-3 cells compared to normal RWPE-1 cells. The promising cytotoxicity of compound **12t** on PC-3 cells motivated us to investigate its effects at cellular level.

2.2.2. Effect of compound **12t** on tubulin polymerization

Tubulin is the principal component of the eukaryotic cytoskeleton and function in several crucial cellular processes including cell replication. As evident from the literature, chalcones shows cytotoxic activity through the inhibition of tubulin polymerization, hence impede with microtubule formation [50]. Moreover, chalcones and curcumin analogues have a great structural resemblance, thus, to investigate the correlation between cytotoxicity of these compounds and tubulin, compound **12t** was examined for its effects on tubulin polymerization in a cell-free *in vitro* assay and nocodazole was chosen as the positive control. Initially, **12t** was screened at 10 μM and % inhibition was found to be 51.8%. As depicted in **Figure 6**, **12t** efficiently inhibited tubulin polymerization in a dose-dependent manner with IC_{50} value of $8.44 \pm 0.13 \mu\text{M}$. These results stipulate that the indicative molecular target of these curcumin analogues might be tubulin.

<Insert Figure 6 here>

2.2.3. Cell cycle analysis

Most of the cytotoxic compounds elicit their growth inhibitory effect either by arresting the cell cycle at a specific checkpoint or by inducing apoptosis [51]. *In vitro* screening results disclosed that compound **12t** showed significant cytotoxicity against PC-3 cells. Therefore, we examined the effect of compound **12t** on cell cycle progression of PC-3 cells by using flow cytometry analysis [52]. The PC-3 cells were treated with 1 μM and 2 μM of compound **12t** for 24 h and stained with propidium iodide. The results from **Figure 7** clearly shows that the ratio of PC-3 cells in G2/M phase was increased from 33.1% in control (DMSO) to 44.6% at 1 μM and 55.8% at 2 μM of **12t**. Concomitantly, there was reduction in the ratio of cells in G0/G1 phase in a dose dependent manner. Henceforth, these results clearly indicate that the treatment of PC-3 cells with **12t** led to G2/M cell cycle arrest.

<Insert Figure 7 here>

2.2.4. Acridine orange-ethidium bromide (AO-EB) staining

The induction of apoptosis by chemotherapeutic agents has always been a preferred choice in the development of new anticancer agents [53]. The morphological changes induced by the most

active compound **12t** in PC-3 cells were further examined by using acridine orange-ethidium bromide (AO-EB) staining to differentiate the live, apoptotic and necrotic cells [54]. AO-EB staining method discerns the live cells from dead cells, because AO permeates the intact cell membrane and stains the cells green, while ethidium bromide can stain only the cells with lost membrane integrity in orange. From **Figure 8**, it can be inferred that the control cells exhibited normal morphology whereas compound **12t** treated PC-3 cells were characterized by the early signs of apoptosis such as condensed chromatin and blebbing of cell membrane at 0.5 μM concentration of compound **12t**. Apoptotic body formation, irregular distribution of chromatin that marginated into horse-shoe shaped nuclei and destructive fragmentation of nuclei were observed at 1 μM and 2 μM respectively.

<Insert Figure 8 here>

2.2.5. Annexin V-FITC/Propidium iodide staining assay

In order to quantify the percentage of cells undergoing apoptosis by the treatment with compound **12t**, Annexin V-FITC/propidium iodide dual staining assay was carried out according to the known procedure. This assay facilitates the detection of live cells (Q1-LL; AV-/PI-), early apoptotic cells (Q2-LR; AV+/PI-), late apoptotic cells (Q3-UR; AV+/PI+) and dead cells (Q4-UL; AV-/PI+). PC-3 cells were treated with 2 μM and 4 μM of compound **12t** for 24 h and stained with Annexin V-FITC/propidium iodide. As shown in **Figure 9**, the compound **12t** increased the percentage of late apoptotic cells [from 5.7% (control) to 27.9% (at 2 μM) and 48.3% (at 4 μM)] which suggests that the compound **12t** induced apoptosis in PC-3 cells in a dose dependent manner.

<Insert Figure 9 here>

2.2.6. DAPI staining

DAPI (4',6-Diamidino-2-phenylindole) is a nuclear stain that strongly binds to adenine-thymine clusters of the minor groove of double-stranded DNA and thus it can visualize nuclear morphological changes. DAPI stains the apoptotic cells bright coloured because of the condensed nucleus which is a characteristic feature of apoptosis. Therefore, DAPI staining was performed as per the procedure available in the literature to detect nuclear damage and chromatin condensation induced by compound **12t** in PC-3 cells. As shown in the **Figure 10**, compound

12t treated PC-3 cells displayed condensed, fragmented and horse-shoe shaped nuclei while the untreated cells exhibited intact nucleus.

<Insert Figure 10 here>

2.2.7. Effect on mitochondrial membrane potential ($D\Psi_m$)

Mitochondria are cellular power house of energy and also plays crucial role in apoptotic processes. As evident from the literature, the damage of mitochondrial membrane integrity, loss or collapse of mitochondrial membrane potential and increase of intracellular ROS levels are closely connected processes that happen during apoptosis [55]. Hence, we tested this possibility by investigating the effect of compound **12t** on $D\Psi_m$ of PC-3 cells using lipophilic cationic JC-1 dye [56]. Healthy polarised mitochondria exhibits red to orange colour because of potential dependent formation of J-aggregates, whereas depolarised mitochondria emits green due to the presence of J-monomers. PC-3 cells were treated with 2 μM and 4 μM of **12t** for 24 h and stained with JC-1 dye. As evident from **Figure 11**, there was increment in depolarised cell population (P2) from 11.9% (control) to 23.67% (at 2 μM) and 52.30% (at 4 μM) in concentration dependent manner. Hence, these results clearly indicate that compound **12t** induced cytotoxicity through mitochondria dependent apoptosis.

<Insert Figure 11 here>

2.2.8. Measurement of reactive oxygen species (ROS) levels

High levels of reactive oxygen species (ROS) causes oxidative damage to mitochondrial permeability transition pore leading to dissipation of mitochondrial membrane potential which further leads to the initiation of intrinsic apoptotic cascade [57]. Hence, we evaluated the elevation of intracellular reactive oxygen species by compound **12t** in PC-3 cells using DCFDA staining method. Treatment with compound **12t** for 6 h resulted in significant increase in DCFDA fluorescence compared to control cells, representing ROS accumulating property of compounds (**Figure 12**), which indicates that compounds induced apoptosis through ROS generation.

<Insert Figure 12 here>

2.3. Molecular docking simulation study

To elucidate the binding mode and type of interactions with tubulin (PDB ID: 1SA0) [58], we have performed molecular docking simulation studies with the most active compound **12t** using the GLIDE docking module of Schrödinger suite 2014-3 [59]. From the docking study, it was observed that the top ranked conformation of compound **12t** was well accommodated inside the colchicine binding site of the tubulin. As shown in **Figure 13a**, docking studies suggest that the compound **12t** binds well in the colchicine-binding domain at the α/β -tubulin interface. More detailed analysis of the inhibitor–tubulin complex (**Figure 13b**) revealed various hydrogen bonding interactions that appear to play a key role in the binding mode. Compound **12t** showed four hydrogen bond interactions with the catalytically active residues Asn101, Gly144, Val181 and Lys254. The nitrogen atom at N-1 position of imidazo[1,2-*a*]pyridine ring acts as hydrogen bond acceptor and involved in the hydrogen bond interaction with back bone NH₂ of Val181 (d = 3.7 Å). The oxygen atom of methoxy group at the second position of chalcone phenyl moiety established two hydrogen bond interactions with side chain NH₂ of Asn101 (d = 1.9 Å) and main chain NH₂ of Gly144 (d = 3.5 Å). Similarly, the oxygen atom of dienone linker showed a hydrogen bonding interaction with the side chain NH₂ of Lys254 (d = 3.6 Å). Additionally, several hydrophobic interactions were observed between the compound **12t** and the active site residues, e.g., Val74, Ala180, Val181, Cys241, Leu242, Leu248, Ala250, Leu252, Leu255, Met259, Val315, Ala316 and Val351 which stabilizes the binding of the compound **12t** in the colchicine-binding domain of α/β -tubulin interface.

<Insert Figure 13 here>

To acquire further intuition, we demonstrated the superimposition of co-crystallized ligand and the best docked pose of compound **12t** in the colchicine binding site of α/β -tubulin interface. The superimposition poses recommended that **12t** occupies the binding pocket in a similar fashion as that of co-crystallized ligand and certainly the 2,4,6-trimethoxy group in **12t** superimposes with the trimethoxy phenyl moiety of colchicine as seen in **Figure 14**. Overall, these molecular docking simulation results provided us a rational justification for why compound **12t** had the good tubulin polymerization inhibitory activity and some important directions for future structural modifications.

<Insert Figure 14 here>

3. Conclusion

In the course of the development of potent cytotoxic agents, a series of some new curcumin inspired imidazo[1,2-*a*]pyridine analogues (**12a–t**) were synthesized and characterized by IR, HRMS, ¹H and ¹³C NMR spectral data. Initially, these compounds were evaluated for their *in vitro* cytotoxic potential on cervical (HeLa), gastric (HGC-27), lung (NCI-H460), prostate (DU-145 and PC-3) and breast (4T1) cancer cell lines and one normal human prostate (RWPE-1) cell line using MTT assay. Among the compounds tested, compounds **12e**, **12r** and **12t** exhibited significant cytotoxicity and **12t** [(1*E*,4*E*)-1-(3-(3,4-difluorophenyl)imidazo[1,2-*a*]pyridin-2-yl)-5-(2,4,6-trimethoxyphenyl)penta-1,4-dien-3-one] being the most active member of the series showed excellent antiproliferative activity on all the tested cell lines, especially PC-3, HGC-27 and HeLa (IC₅₀ of 2.11 ± 0.27 μM, 2.21 ± 0.25 μM, 2.53 ± 0.01 μM respectively). Interestingly, the most active compound **12t** was found to be less cytotoxic on normal human prostate (RWPE-1) cells and almost 2 times more selective on PC-3 cells. The results from aqueous solubility test showed that compounds **12e** and **12t** have 1.7 and 2.8 times more aqueous solubility than curcumin. Moreover, compound **12t** efficiently inhibited tubulin polymerization with IC₅₀ value of 8.44 ± 0.13 μM and molecular modelling studies disclosed that **12t** binds at the colchicine binding site of the tubulin. Also, **12t** arrests PC-3 cells in G2/M phase as evident from the cell cycle analysis. Further, treatment of PC-3 cells with **12t** displayed typical apoptotic morphology, also led to the impairment of mitochondrial membrane potential (DΨ_m) and increased levels of reactive oxygen species (ROS). Overall, the results from acridine orange/ethidium bromide (AO-EB) and DAPI staining studies, annexin V-FITC/propidium iodide staining assay, analysis of mitochondrial membrane potential (DΨ_m) and reactive oxygen species (ROS) levels certainly demonstrated the induction of apoptosis in PC-3 cells by compound **12t**. In conclusion, curcumin inspired imidazo[1,2-*a*]pyridine analogues described in the present work indicate exciting possibilities of developing new cancer therapeutics *via* their structural modifications.

4. Experimental section

4.0. General

All the chemicals, reagents, starting materials and solvents were procured from commercial suppliers and were used without further purification. Analytical thin layer chromatography (TLC) was performed using MERCK[®] pre-coated silica gel 60-F-254 (0.5 mm) aluminum plates. Visualization of spots on TLC plates was achieved by UV light. Wherever required, column chromatography was performed with silica gel (60-120 mesh) or neutral alumina. Ethyl acetate and hexane were used as eluents. Melting points were checked using Stuart digital SMP 30 melting point apparatus and were uncorrected. FT-IR spectra for all the compounds were recorded on a Perkin Elmer instrument by using ATR method. ¹H and ¹³C NMR spectra were recorded on an Avance NMR instrument operated at 500 and 125 MHz respectively using tetra methyl silane (TMS) as the internal reference. Chemical shift values were given in ppm and *J* values were documented in Hertz. Spin multiplicities were explained as s (singlet), d (doublet), t (triplet), dd (doublet of doublet), q (quartet) and m (multiplet). HRMS were obtained with Agilent QTOF mass spectrometer 6540 series instrument and were performed in the ESI technique at 70 eV.

4.1. Synthetic procedures and spectral data

4.1.1. General synthetic procedure for the synthesis of chalcones **3**

To a magnetically stirred solution of substituted benzaldehyde (**1**, 1 mmol) in ethanol (3 mL) were added 0.5 mL of acetone and 1 mL of 15% aqueous NaOH (1 mL) solution at 0 °C. The reaction was allowed to stir at room temperature till it was completed. The reaction mixture was evaporated to dryness, extracted twice with ethyl acetate, the combined organic layers were dried over anhydrous Na₂SO₄ and concentrated under vacuum. The crude residue was purified by column chromatography (Silica gel, 60-120 mesh, 9:1 hexane/ethyl acetate) to afford the desired chalcone (**3**) in good to very good yields.

4.1.2. General synthetic procedure for the synthesis of **6**

A solution of 2-amino pyridine (**4**, 1 mmol) and ethyl bromopyruvate (**5**, 1.2 mmol) in ethanol (15 mL) was stirred under reflux for 1 h, and concentrated in vacuo to remove the solvent. The residue was partitioned between dichloromethane (15 mL) and saturated aqueous solution of sodium carbonate (10 mL). The organic layer was separated, dried over anhydrous Na₂SO₄ and concentrated under reduced pressure. The residue was purified by column chromatography on

neutral alumina to afford imidazo[1,2-*a*]pyridine-2-carboxylic acid ethyl ester as a light brown solid (**6**) in good yield.

4.1.3. General procedure for the synthesis of **7**

N-Iodosuccinimide (1.5 mmol) was added to a magnetically stirred solution of imidazo[1,2-*a*]pyridine-2-carboxylic acid ethyl ester (**6**, 1 mmol) in dry CH₃CN (5 mL). The reaction mixture was stirred at rt for 1 h. The filtrate was concentrated to remove the solvent, and the residue was purified by column chromatography on neutral alumina to afford ethyl 3-iodoimidazo[1,2-*a*]pyridine-2-carboxylate (**7**) in moderate yield.

4.1.4. General procedure for the synthesis of **9**

To a mixture of ethyl 3-iodoimidazo[1,2-*a*]pyridine-2-carboxylate (**7**, 1 mmol) and Pd(PPh₃)₄ (0.05 mmol) in dioxane (8 mL) was added the corresponding phenyl boronic acid (1.1 mmol) followed by the addition of sodium carbonate (2 mmol) in water (2 mL). The reaction mixture was heated at 75 °C with vigorous stirring under nitrogen atmosphere, and the reaction was monitored by TLC. After the aryl halide (**7**) was consumed completely, the reaction mixture was concentrated to remove the solvent and then extracted with dichloromethane (2 x 20 mL). The combined organic extracts were washed with water (20 mL), dried over anhydrous Na₂SO₄, and concentrated to dryness under vacuo. The crude product (**9**) was purified by column chromatography on neutral alumina.

4.1.5. General procedure for the synthesis of **10**

To a slurry of lithium aluminium hydride (2 mmol) in anhydrous tetrahydrofuran (3 mL), which was cooled to 0 °C, was added a solution of ethyl 3-arylimidazo[1,2-*a*]pyridine-2-carboxylate (**9**, 1 mmol) in anhydrous tetrahydrofuran (2 mL) dropwise. After being stirred at 0 °C for 1 h, the reaction was quenched by adding 1N aqueous solution of hydrochloride (0.8 mL) slowly. After being stirred for 10 min, the mixture was basified by the addition of saturated aqueous solution of sodium bicarbonate (1 mL), and filtered through celite. The filter cake was washed with dichloromethane (10 mL). The organic layer was separated and the aqueous layer was extracted with dichloromethane (2 x 10 mL). The organic layers were combined, dried over anhydrous Na₂SO₄ and concentrated under reduced pressure. The residue was purified by column

chromatography on neutral alumina to afford (3-arylimidazo[1,2-*a*]pyridin-2-yl)methanol (**10**) in moderate to good yields.

4.1.6. General procedure for the synthesis of **11**

To a magnetically stirred solution of **10** (1 mmol) in DCM (10 mL) at 0 °C were added water (100 µL) and Dess-Martin periodinane (2.5 mmol) sequentially. The reaction was monitored by TLC until the alcohol was consumed. The reaction mixture was filtered through a cartridge of SiO₂ (eluting with Et₂O) and solvent was removed in vacuo. The residue was purified by column chromatography on neutral alumina to afford 3-arylimidazo[1,2-*a*]pyridin-2-carbaldehyde (**11**) in moderate to good yields.

4.1.7. General procedure for the synthesis of **12a-t**

To a stirred solution of chalcone **3** (0.5 mmol) in ethanol (5 mL) was added 15% aqueous CH₃ONa (1-2 mL) solution and aldehyde **11** (0.5 mmol) at 0 °C. The resulting solution was stirred at room temperature till the reaction was completed. The reaction mixture was evaporated to dryness, partitioned between ethyl acetate and water, the combined organic layers were dried over anhydrous Na₂SO₄ and concentrated under reduced pressure. The crude mass was purified either by recrystallization in ethanol or by column chromatography on neutral alumina to furnish the final compounds **12a-t** in moderate to very good yields.

4.1.8. Spectral data

4.1.8.1. (1*E*,4*E*)-1-(4-methoxyphenyl)-5-(3-phenylimidazo[1,2-*a*]pyridin-2-yl)penta-1,4-dien-3-one (**12a**)

Yellow solid, yield 73.1%; mp: 152–153 °C; FT-IR (cm⁻¹): 3047.4, 2932.3, 1651.8, 1620.5, 1510.8, 1450.3, 1352.2, 1249.9, 1096.5, 763.0; ¹H NMR (500 MHz, CDCl₃): δ 8.10 (d, *J* = 6.9 Hz, 1H), 7.77 (s, 1H), 7.73 (d, *J* = 7.0 Hz, 2H), 7.66 (d, *J* = 9.1 Hz, 1H), 7.63 – 7.43 (m, 8H), 6.93 (d, *J* = 8.6 Hz, 2H), 6.88 (d, *J* = 16.1 Hz, 1H), 6.78 (t, *J* = 6.7 Hz, 1H), 3.85 (s, 3H); ¹³C NMR (125 MHz, CDCl₃): δ 189.0, 161.5, 145.5, 143.0, 139.1, 133.2, 130.2, 130.1, 129.5, 129.3, 127.7, 127.6, 126.3, 125.9, 125.1, 123.6, 117.8, 114.4, 112.8, 55.4; HRMS (ESI): *m/z* calcd for C₂₅H₂₁N₂O₂ 381.1598, found 381.1606 [M+H]⁺.

4.1.8.2. (1E,4E)-1-(2,4-dimethoxyphenyl)-5-(3-phenylimidazo[1,2-a]pyridin-2-yl)penta-1,4-dien-3-one (**12b**)

Yellow solid, yield 68.7%; mp: 141–142 °C; FT-IR (cm⁻¹): 2935.0, 1644.6, 1600.7, 1503.2, 1454.9, 1348.8, 1290.9, 1094.7, 751.4; ¹H NMR (500 MHz, CDCl₃): δ 8.10 (d, *J* = 6.9 Hz, 1H), 8.02 (d, *J* = 16.2 Hz, 1H), 7.74 (d, *J* = 1.1 Hz, 2H), 7.66 (d, *J* = 9.2 Hz, 1H), 7.58 (d, *J* = 7.0 Hz, 2H), 7.54 – 7.43 (m, 5H), 7.03 (d, *J* = 16.2 Hz, 1H), 6.77 (t, *J* = 6.5 Hz, 1H), 6.53 (d, *J* = 8.6, 2.2 Hz, 1H), 6.47 (d, *J* = 2.1 Hz, 1H), 3.89 (s, 3H), 3.85 (s, 3H); ¹³C NMR (125 MHz, CDCl₃): δ 189.6, 162.9, 160.2, 145.5, 139.2, 138.8, 132.8, 130.8, 130.2, 129.5, 129.2, 127.6, 127.5, 126.4, 126.2, 125.7, 123.6, 117.7, 117.1, 112.7, 105.4, 98.4, 55.5, 55.4; HRMS (ESI): *m/z* calcd for C₂₆H₂₃N₂O₃ 411.1703, found 411.1712 [M+H]⁺.

4.1.8.3. (1E,4E)-1-(2,5-dimethoxyphenyl)-5-(3-phenylimidazo[1,2-a]pyridin-2-yl)penta-1,4-dien-3-one (**12c**)

Yellow solid, yield 63.3%; mp: 129–130 °C; FT-IR (cm⁻¹): 2930.1, 1663.4, 1618.9, 1535.6, 1461.8, 1350.2, 1291.9, 1091.1, 751.3; ¹H NMR (500 MHz, CDCl₃): δ 8.11 – 8.07 (m, 1H), 8.04 (s, 1H), 7.75 (s, 2H), 7.67 (d, *J* = 9.2 Hz, 1H), 7.63 – 7.42 (m, 6H), 7.12 (d, *J* = 3.0 Hz, 1H), 7.07 (d, *J* = 16.3 Hz, 1H), 6.93 (dd, *J* = 9.0, 3.0 Hz, 1H), 6.87 (d, *J* = 9.0 Hz, 1H), 6.78 (t, *J* = 6.8 Hz, 1H), 3.87 (s, 3H), 3.80 (s, 3H); ¹³C NMR (125 MHz, CDCl₃): δ 189.5, 153.5, 153.2, 145.5, 139.1, 138.4, 133.4, 130.2, 129.5, 129.3, 128.2, 127.6, 126.3, 125.9, 124.4, 123.7, 117.8, 117.6, 113.1, 112.8, 112.4, 56.0, 55.8; HRMS (ESI): *m/z* calcd for C₂₆H₂₃N₂O₃ 411.1703, found 411.1709 [M+H]⁺.

4.1.8.4. (1E,4E)-1-(3,4-dimethoxyphenyl)-5-(3-phenylimidazo[1,2-a]pyridin-2-yl)penta-1,4-dien-3-one (**12d**)

Yellow solid, yield 79.2%; mp: 102–104 °C; FT-IR (cm⁻¹): 2936.6, 1668.0, 1650.2, 1621.4, 1507.3, 1466.0, 1348.9, 1265.0, 1101.4, 751.1; ¹H NMR (500 MHz, CDCl₃): δ 8.10 (d, *J* = 7.0 Hz, 1H), 7.79 – 7.71 (m, 3H), 7.66 (d, *J* = 9.1 Hz, 1H), 7.59 (t, *J* = 7.3 Hz, 2H), 7.52 (dd, *J* = 9.1, 7.9 Hz, 3H), 7.31 – 7.27 (m, 1H), 7.19 (dd, *J* = 8.3, 1.6 Hz, 1H), 7.14 (d, *J* = 1.6 Hz, 1H), 6.89 (dd, *J* = 16.2, 8.2 Hz, 2H), 6.78 (t, *J* = 6.8 Hz, 1H), 3.94 (s, 3H), 3.93 (s, 3H); ¹³C NMR (125 MHz, CDCl₃): δ 188.9, 151.3, 149.2, 145.5, 143.2, 139.0, 133.3, 130.2, 129.5, 129.3, 127.9, 127.7, 127.5, 126.3, 125.7, 125.5, 123.7, 123.1, 117.8, 112.8, 111.1, 109.7, 56.0, 55.9; HRMS (ESI): *m/z* calcd for C₂₆H₂₃N₂O₃ 411.1703, found 411.1712 [M+H]⁺.

4.1.8.5. (1E,4E)-1-(3-phenylimidazo[1,2-a]pyridin-2-yl)-5-(2,4,5-trimethoxyphenyl)penta-1,4-dien-3-one (**12e**)

Yellow solid, yield 73.5%; mp: 244–246 °C; FT-IR (cm⁻¹): 3046.2, 1657.3, 1601.0, 1505.1, 1447.6, 1349.3, 1284.1, 1094.7, 754.1; ¹H NMR (500 MHz, CDCl₃): δ 8.13 – 8.02 (m, 2H), 7.75 (s, 2H), 7.66 (d, *J* = 9.2 Hz, 1H), 7.64 – 7.55 (m, 3H), 7.54 – 7.47 (m, 3H), 7.09 (s, 1H), 6.96 (d, *J* = 16.2 Hz, 1H), 6.78 (t, *J* = 6.8 Hz, 1H), 6.51 (s, 1H), 3.94 (s, 3H), 3.90 (s, 3H), 3.88 (s, 3H); ¹³C NMR (125 MHz, CDCl₃): δ 189.4, 154.3, 152.3, 145.5, 143.2, 139.2, 138.3, 132.9, 130.2, 129.5, 129.2, 127.7, 127.6, 126.2, 126.0, 125.7, 123.6, 117.7, 115.4, 112.7, 110.8, 96.7, 56.3, 56.2, 56.0; HRMS (ESI): *m/z* calcd for C₂₇H₂₅N₂O₄ 441.1809, found 441.1813 [M+H]⁺.

4.1.8.6. (1E,4E)-1-(3-phenylimidazo[1,2-a]pyridin-2-yl)-5-(2,4,6-trimethoxyphenyl)penta-1,4-dien-3-one (**12f**)

Yellow solid, yield 76.7%; mp: 202–205 °C; FT-IR (cm⁻¹): 2972.0, 1660.1, 1598.7, 1554.4, 1469.1, 1350.9, 1285.2, 1090.9, 752.1; ¹H NMR (500 MHz, CDCl₃): δ 8.20 (d, *J* = 16.2 Hz, 1H), 8.10 (d, *J* = 6.9 Hz, 1H), 7.76 – 7.62 (m, 3H), 7.60 – 7.55 (m, 2H), 7.51 (d, *J* = 7.3 Hz, 3H), 7.42 (d, *J* = 16.2 Hz, 1H), 7.27 – 7.20 (m, 1H), 6.76 (dd, *J* = 9.8, 3.8 Hz, 1H), 6.12 (s, 2H), 3.88 (s, 6H), 3.85 (s, 3H); ¹³C NMR (125 MHz, CDCl₃): δ 190.5, 163.0, 161.6, 145.4, 139.4, 134.5, 132.1, 130.2, 129.4, 129.1, 127.7, 127.6, 127.3, 127.0, 126.1, 123.6, 117.7, 112.6, 106.4, 90.4, 55.7, 55.4; HRMS (ESI): *m/z* calcd for C₂₇H₂₅N₂O₄ 441.1809, found 441.1813 [M+H]⁺.

4.1.8.7. (1E,4E)-1-(4-methoxyphenyl)-5-(3-(3-methoxyphenyl)imidazo[1,2-a]pyridin-2-yl)penta-1,4-dien-3-one (**12g**)

Yellow solid, yield 64.8%; mp: 113–114 °C; FT-IR (cm⁻¹): 2969.6, 1647.1, 1599.9, 1509.7, 1422.1, 1346.0, 1288.4, 1091.7, 754.0; ¹H NMR (500 MHz, CDCl₃): δ 8.12 (d, *J* = 6.9 Hz, 1H), 7.81 – 7.67 (m, 3H), 7.66 (d, *J* = 9.1 Hz, 1H), 7.56 (d, *J* = 8.6 Hz, 2H), 7.50 (t, *J* = 7.9 Hz, 1H), 7.29 – 7.24 (m, 1H), 7.11 – 7.04 (m, 2H), 7.02 (s, 1H), 6.93 (d, *J* = 8.6 Hz, 2H), 6.88 (d, *J* = 16.1 Hz, 1H), 6.78 (t, *J* = 6.7 Hz, 1H), 3.88 (s, 3H), 3.85 (s, 3H); ¹³C NMR (125 MHz, CDCl₃): δ 189.0, 161.5, 160.3, 145.5, 143.0, 139.1, 133.2, 130.6, 130.1, 128.8, 127.6, 127.5, 126.3, 125.9, 125.1, 123.8, 122.5, 117.8, 115.7, 114.8, 114.4, 112.7, 55.5, 55.4; HRMS (ESI): *m/z* calcd for C₂₆H₂₃N₂O₃ 411.1703, found 411.1709 [M+H]⁺.

4.1.8.8. (1E,4E)-1-(2,4-dimethoxyphenyl)-5-(3-(3-methoxyphenyl)imidazo[1,2-a]pyridin-2-yl)penta-1,4-dien-3-one (**12h**)

Yellow solid, yield 76.4%; mp: 138–140 °C; FT-IR (cm⁻¹): 2972.2, 1662.4, 1597.5, 1505.4, 1466.1, 1335.1, 1275.2, 1099.4, 751.9; ¹H NMR (500 MHz, CDCl₃): δ 8.12 (d, *J* = 6.9 Hz, 1H), 8.02 (d, *J* = 16.2 Hz, 1H), 7.81 – 7.69 (m, 2H), 7.66 (d, *J* = 9.1 Hz, 1H), 7.55 – 7.45 (m, 2H), 7.27 – 7.23 (m, 1H), 7.09 (d, *J* = 7.5 Hz, 1H), 7.07 – 7.00 (m, 3H), 6.77 (d, *J* = 6.8 Hz, 1H), 6.53 (dd, *J* = 8.6, 2.2 Hz, 1H), 6.47 (d, *J* = 2.1 Hz, 1H), 3.89 (s, 3H), 3.87 (s, 3H), 3.85 (s, 3H); ¹³C NMR (125 MHz, CDCl₃): δ 189.5, 162.9, 160.3, 145.5, 139.2, 138.8, 132.8, 130.7, 130.5, 128.8, 127.3, 126.4, 126.2, 125.7, 123.8, 122.5, 117.7, 117.1, 115.7, 114.8, 112.7, 105.3, 98.4, 55.5, 55.4; HRMS (ESI): *m/z* calcd for C₂₇H₂₅N₂O₄ 441.1809, found 441.1813 [M+H]⁺.

4.1.8.9. (1E,4E)-1-(2,5-dimethoxyphenyl)-5-(3-(3-methoxyphenyl)imidazo[1,2-a]pyridin-2-yl)penta-1,4-dien-3-one (**12i**)

Yellow solid, yield 67.3%; mp: 170–171 °C; FT-IR (cm⁻¹): 2971.8, 1648.7, 1587.2, 1493.8, 1348.9, 1286.3, 1092.3, 750.2; ¹H NMR (500 MHz, CDCl₃): δ 8.12 (d, *J* = 6.9 Hz, 1H), 8.06 (d, *J* = 16.3 Hz, 1H), 7.76 (q, *J* = 15.3 Hz, 2H), 7.66 (d, *J* = 9.1 Hz, 1H), 7.50 (t, *J* = 7.9 Hz, 1H), 7.28 – 7.24 (m, 1H), 7.14 – 7.04 (m, 4H), 7.02 (s, 1H), 6.93 (dd, *J* = 9.0, 2.9 Hz, 1H), 6.86 (d, *J* = 9.0 Hz, 1H), 6.78 (t, *J* = 6.8 Hz, 1H), 3.88 (s, 3H), 3.87 (s, 3H), 3.80 (s, 3H); ¹³C NMR (125 MHz, CDCl₃): δ 189.5, 160.3, 153.5, 153.2, 145.5, 139.1, 138.4, 133.4, 130.6, 128.8, 128.1, 127.5, 126.3, 125.9, 124.4, 123.8, 122.5, 117.8, 117.5, 115.7, 114.9, 113.1, 112.7, 112.4, 56.0, 55.8, 55.4; HRMS (ESI): *m/z* calcd for C₂₇H₂₅N₂O₄ 441.1809, found 441.1817 [M+H]⁺.

4.1.8.10. (1E,4E)-1-(3,4-dimethoxyphenyl)-5-(3-(3-methoxyphenyl)imidazo[1,2-a]pyridin-2-yl)penta-1,4-dien-3-one (**12j**)

Yellow solid, yield 77.2%; mp: 170–172 °C; FT-IR (cm⁻¹): 2967.8, 1642.2, 1621.6, 1600.3, 1510.1, 1465.5, 1358.0, 1295.9, 1088.1, 750.3; ¹H NMR (500 MHz, CDCl₃): δ 8.11 (d, *J* = 7.0 Hz, 1H), 7.80 – 7.70 (m, 3H), 7.65 (d, *J* = 9.2 Hz, 1H), 7.50 (t, *J* = 7.9 Hz, 1H), 7.28 – 7.24 (m, 1H), 7.19 (dd, *J* = 8.3, 1.4 Hz, 1H), 7.14 (s, 1H), 7.11 – 7.04 (m, 2H), 7.02 (s, 1H), 6.92 – 6.85 (m, 2H), 6.78 (t, *J* = 6.8 Hz, 1H), 3.94 (s, 3H), 3.93 (s, 3H), 3.88 (s, 3H); ¹³C NMR (125 MHz, CDCl₃): δ 188.9, 160.3, 151.3, 149.2, 145.4, 143.2, 139.0, 133.3, 130.5, 128.7, 127.9, 127.5,

126.3, 125.7, 125.5, 123.8, 123.0, 122.5, 117.7, 115.7, 114.8, 112.8, 111.1, 109.7, 56.0, 55.8, 55.4; HRMS (ESI): m/z calcd for $C_{27}H_{25}N_2O_4$ 441.1809, found 441.1818 $[M+H]^+$.

4.1.8.11. (1*E*,4*E*)-1-(4-methoxyphenyl)-5-(3-(4-methoxyphenyl)imidazo[1,2-*a*]pyridin-2-yl)penta-1,4-dien-3-one (**12k**)

Yellow solid, yield 63.7%; mp: 126–128 °C; FT-IR (cm^{-1}): 2988.5, 1654.7, 1590.0, 1509.5, 1347.2, 1300.1, 1249.9, 1081.9, 750.3; 1H NMR (500 MHz, $CDCl_3$): δ 8.06 (d, $J = 6.9$ Hz, 1H), 7.80 – 7.75 (m, 1H), 7.72 (s, 2H), 7.67 (d, $J = 8.9$ Hz, 1H), 7.56 (d, $J = 8.7$ Hz, 2H), 7.43 (d, $J = 8.4$ Hz, 2H), 7.30 – 7.27 (m, 1H), 7.13 – 7.08 (m, 2H), 6.93 (d, $J = 8.6$ Hz, 2H), 6.87 (d, $J = 16.1$ Hz, 1H), 6.79 (t, $J = 6.8$ Hz, 1H), 3.91 (s, 3H), 3.85 (s, 3H); ^{13}C NMR (125 MHz, $CDCl_3$): δ 189.0, 161.5, 160.4, 145.4, 142.9, 138.9, 133.4, 131.6, 130.0, 128.5, 127.7, 126.1, 125.6, 125.2, 123.7, 119.6, 117.7, 115.0, 114.4, 112.6, 55.5, 55.4; HRMS (ESI): m/z calcd for $C_{26}H_{23}N_2O_3$ 411.1703, found 411.1706 $[M+H]^+$.

4.1.8.12. (1*E*,4*E*)-1-(2,4-dimethoxyphenyl)-5-(3-(4-methoxyphenyl)imidazo[1,2-*a*]pyridin-2-yl)penta-1,4-dien-3-one (**12l**)

Yellow solid, yield 69.5%; mp: 165–166 °C; FT-IR (cm^{-1}): 2988.2, 1644.4, 1590.0, 1503.2, 1455.6, 1345.6, 1289.5, 1091.5, 762.5; 1H NMR (500 MHz, $CDCl_3$): δ 8.02 (d, $J = 17.5$ Hz, 2H), 7.73 – 7.40 (m, 6H), 7.25 – 7.18 (m, 1H), 7.10 (d, $J = 7.3$ Hz, 2H), 7.02 (d, $J = 16.0$ Hz, 1H), 6.81 – 6.72 (m, 1H), 6.53 (d, $J = 6.7$ Hz, 1H), 6.47 (s, 1H), 3.91 (s, 3H), 3.89 (s, 3H), 3.85 (s, 3H); ^{13}C NMR (125 MHz, $CDCl_3$): δ 189.6, 162.9, 160.3, 160.2, 145.3, 139.0, 138.7, 133.0, 132.1, 131.5, 130.7, 128.5, 128.4, 127.5, 126.0, 125.8, 123.6, 119.6, 117.7, 117.1, 115.0, 112.6, 105.3, 98.4, 55.5, 55.4; HRMS (ESI): m/z calcd for $C_{27}H_{25}N_2O_4$ 441.1809, found 441.1815 $[M+H]^+$.

4.1.8.13. (1*E*,4*E*)-1-(2,5-dimethoxyphenyl)-5-(3-(4-methoxyphenyl)imidazo[1,2-*a*]pyridin-2-yl)penta-1,4-dien-3-one (**12m**)

Yellow solid, yield 63.0%; mp: 96–98 °C; FT-IR (cm^{-1}): 2971.3, 1645.5, 1610.4, 1492.8, 1347.3, 1286.6, 1089.8, 753.5; 1H NMR (500 MHz, $CDCl_3$): δ 8.08 (d, $J = 15.9$ Hz, 2H), 7.81 – 7.51 (m, 4H), 7.50 – 7.30 (m, 3H), 7.15 – 7.03 (m, 3H), 6.93 (d, $J = 6.4$ Hz, 1H), 6.86 (d, $J = 8.8$ Hz, 1H), 6.82 – 6.76 (m, 1H), 3.91 (s, 3H), 3.87 (s, 3H), 3.81 (s, 3H); ^{13}C NMR (125 MHz, $CDCl_3$): δ

189.5, 160.4, 153.5, 153.2, 145.4, 138.9, 138.3, 133.6, 131.6, 128.2, 127.8, 126.1, 125.5, 124.4, 123.7, 119.5, 117.7, 117.5, 115.0, 113.1, 112.6, 112.4, 56.0, 55.8, 55.4; HRMS (ESI): m/z calcd for $C_{27}H_{25}N_2O_4$ 441.1809, found 441.1813 $[M+H]^+$.

4.1.8.14. (1*E*,4*E*)-1-(3,4-dimethoxyphenyl)-5-(3-(4-methoxyphenyl)imidazo[1,2-*a*]pyridin-2-yl)penta-1,4-dien-3-one (**12n**)

Yellow solid, yield 65.4%; mp: 116–118 °C; FT-IR (cm^{-1}): 2988.6, 1656.2, 1620.1, 1508.3, 1439.4, 1248.6, 1101.9, 752.0; 1H NMR (500 MHz, $CDCl_3$): δ 8.05 (d, $J = 6.9$ Hz, 1H), 7.76 (s, 1H), 7.73 (d, $J = 2.9$ Hz, 2H), 7.65 (d, $J = 9.1$ Hz, 1H), 7.43 (d, $J = 8.6$ Hz, 2H), 7.25 – 7.22 (m, 1H), 7.19 (d, $J = 8.2$ Hz, 1H), 7.16 – 7.07 (m, 3H), 6.92 – 6.85 (m, 2H), 6.77 (t, $J = 6.7$ Hz, 1H), 3.94 (s, 3H), 3.93 (s, 3H), 3.91 (s, 3H); ^{13}C NMR (125 MHz, $CDCl_3$): δ 188.9, 160.4, 151.3, 149.2, 145.4, 143.1, 138.9, 133.5, 131.6, 127.9, 127.8, 126.1, 125.6, 125.3, 123.7, 123.0, 119.5, 117.7, 115.0, 112.6, 111.1, 109.7, 56.0, 55.8, 55.5; HRMS (ESI): m/z calcd for $C_{27}H_{25}N_2O_4$ 441.1809, found 441.1814 $[M+H]^+$.

4.1.8.15. (1*E*,4*E*)-1-(3-(4-methoxyphenyl)imidazo[1,2-*a*]pyridin-2-yl)-5-(2,4,5-trimethoxyphenyl)penta-1,4-dien-3-one (**12o**)

Yellow solid, yield 63.8%; mp: 194–195 °C; FT-IR (cm^{-1}): 2971.0, 1658.7, 1606.0, 1507.5, 1463.7, 1349.2, 1282.8, 1090.3, 751.9; 1H NMR (500 MHz, $CDCl_3$): δ 8.13 – 8.05 (m, 2H), 7.83 – 7.66 (m, 4H), 7.43 (d, $J = 8.5$ Hz, 2H), 7.15 – 7.07 (m, 3H), 6.96 (d, $J = 16.2$ Hz, 1H), 6.80 (t, $J = 6.8$ Hz, 1H), 6.51 (s, 1H), 3.94 (s, 3H), 3.91 (s, 6H), 3.89 (s, 3H); ^{13}C NMR (125 MHz, $CDCl_3$): δ 189.4, 160.4, 154.3, 152.3, 145.3, 143.3, 139.0, 138.2, 133.0, 131.6, 127.6, 126.0, 125.8, 125.7, 123.7, 119.6, 117.7, 115.4, 115.0, 112.6, 110.9, 96.7, 56.3, 56.2, 56.0, 55.4; HRMS (ESI): m/z calcd for $C_{28}H_{27}N_2O_5$ 471.1914, found 471.1919 $[M+H]^+$.

4.1.8.16. (1*E*,4*E*)-1-(3-(3,4-difluorophenyl)imidazo[1,2-*a*]pyridin-2-yl)-5-(4-methoxyphenyl)penta-1,4-dien-3-one (**12p**)

Yellow solid, yield 71.9%; mp: 136–138 °C; FT-IR (cm^{-1}): 2988.5, 1651.7, 1600.8, 1511.1, 1495.6, 1346.0, 1306.5, 1115.5, 752.4; 1H NMR (500 MHz, $CDCl_3$): δ 8.02 (d, $J = 6.9$ Hz, 1H), 7.79 – 7.64 (m, 4H), 7.56 (d, $J = 8.6$ Hz, 2H), 7.44 – 7.28 (m, 3H), 6.94 (d, $J = 8.7$ Hz, 2H), 6.89 (s, 1H), 6.84 (dd, $J = 12.7, 6.0$ Hz, 2H), 3.85 (s, 3H); ^{13}C NMR (125 MHz, $CDCl_3$): δ 188.8,

161.6, 145.6, 143.3, 139.5, 132.3, 130.1, 127.5, 126.9, 126.6, 126.5, 125.1, 125.0, 124.5, 123.3, 119.2, 119.1, 118.8, 118.6, 117.9, 114.4, 113.2, 55.4; HRMS (ESI): m/z calcd for $C_{25}H_{19}F_2N_2O_2$ 417.1409, found 417.1406 $[M+H]^+$.

4.1.8.17. *(1E,4E)-1-(3-(3,4-difluorophenyl)imidazo[1,2-a]pyridin-2-yl)-5-(2,4-dimethoxyphenyl)penta-1,4-dien-3-one (12q)*

Yellow solid, yield 73.0%; mp: 195–196 °C; FT-IR (cm^{-1}): 2972.3, 1639.7, 1602.6, 1503.6, 1454.2, 1346.7, 1305.0, 1140.4, 756.3; 1H NMR (500 MHz, $CDCl_3$): δ 8.06 – 7.99 (m, 2H), 7.74 (d, $J = 15.2$ Hz, 1H), 7.70 – 7.63 (m, 2H), 7.53 (d, $J = 8.6$ Hz, 1H), 7.44 – 7.27 (m, 4H), 7.02 (d, $J = 16.2$ Hz, 1H), 6.82 (t, $J = 6.8$ Hz, 1H), 6.53 (dd, $J = 8.6, 2.2$ Hz, 1H), 6.47 (d, $J = 2.2$ Hz, 1H), 3.90 (s, 3H), 3.85 (s, 3H); ^{13}C NMR (125 MHz, $CDCl_3$): δ 189.4, 163.0, 160.3, 145.6, 139.6, 139.1, 131.8, 130.8, 127.0, 126.9, 126.5, 125.6, 124.9, 124.5, 123.2, 119.2, 119.1, 118.8, 118.6, 117.9, 117.0, 113.1, 105.4, 98.4, 55.5, 55.4; HRMS (ESI): m/z calcd for $C_{26}H_{21}F_2N_2O_3$ 447.1515, found 447.1519 $[M+H]^+$.

4.1.8.18. *(1E,4E)-1-(3-(3,4-difluorophenyl)imidazo[1,2-a]pyridin-2-yl)-5-(2,5-dimethoxyphenyl)penta-1,4-dien-3-one (12r)*

Yellow solid, yield 79.7%; mp: 177–179 °C; FT-IR (cm^{-1}): 2988.3, 1667.5, 1617.8, 1493.4, 1349.1, 1289.6, 1092.9, 1025.9, 748.2; 1H NMR (500 MHz, $CDCl_3$): δ 8.07 (d, $J = 16.3$ Hz, 1H), 8.03 (d, $J = 6.9$ Hz, 1H), 7.76 (d, $J = 15.2$ Hz, 1H), 7.70 – 7.65 (m, 2H), 7.44 – 7.27 (m, 4H), 7.12 (d, $J = 3.0$ Hz, 1H), 7.06 (d, $J = 16.3$ Hz, 1H), 6.94 (dd, $J = 9.0, 3.0$ Hz, 1H), 6.87 (d, $J = 9.0$ Hz, 1H), 6.83 (t, $J = 6.8$ Hz, 1H), 3.87 (s, 3H), 3.81 (s, 3H); ^{13}C NMR (125 MHz, $CDCl_3$): δ 189.3, 153.5, 153.2, 145.6, 139.5, 138.7, 132.5, 128.1, 126.9, 126.6, 126.5, 125.2, 124.5, 124.3, 123.3, 119.2, 119.1, 118.8, 118.6, 117.9, 117.7, 113.2, 113.1, 112.4, 56.0, 55.8; HRMS (ESI): m/z calcd for $C_{26}H_{21}F_2N_2O_3$ 447.1515, found 447.1522 $[M+H]^+$.

4.1.8.19. *(1E,4E)-1-(3-(3,4-difluorophenyl)imidazo[1,2-a]pyridin-2-yl)-5-(3,4-dimethoxyphenyl)penta-1,4-dien-3-one (12s)*

Yellow solid, yield 82.0%; mp: 180–182 °C; FT-IR (cm^{-1}): 2959.0, 1658.2, 1617.3, 1508.1, 1469.7, 1347.6, 1285.2, 1107.3; 1H NMR (500 MHz, $CDCl_3$): δ 8.03 (d, $J = 6.9$ Hz, 1H), 7.75 (d, $J = 15.5$ Hz, 2H), 7.71 – 7.63 (m, 2H), 7.44 – 7.28 (m, 3H), 7.20 (dd, $J = 8.3, 1.5$ Hz, 1H), 7.14

(s, 1H), 6.97 – 6.87 (m, 2H), 6.84 (dd, $J = 12.7, 5.8$ Hz, 2H), 3.94 (s, 3H), 3.93 (s, 3H); ^{13}C NMR (125 MHz, CDCl_3): δ 188.7, 151.4, 149.2, 145.6, 143.5, 139.5, 132.3, 127.7, 126.9, 126.6, 126.3, 125.4, 125.2, 124.4, 123.3, 123.1, 119.2, 119.1, 118.8, 118.7, 117.9, 113.2, 111.1, 109.7, 56.0, 55.8; HRMS (ESI): m/z calcd for $\text{C}_{26}\text{H}_{21}\text{F}_2\text{N}_2\text{O}_3$ 447.1515, found 447.1519 $[\text{M}+\text{H}]^+$.

4.1.8.20. *(1E,4E)-1-(3-(3,4-difluorophenyl)imidazo[1,2-a]pyridin-2-yl)-5-(2,4,6-trimethoxyphenyl)penta-1,4-dien-3-one (12t)*

Yellow solid, yield 67.5%; mp: 240–241 °C; FT-IR (cm^{-1}): 2972.0, 1658.6, 1639.2, 1621.3, 1601.2, 1511.2, 1465.4, 1351.1, 1294.5, 1099.7, 752.5; ^1H NMR (500 MHz, CDCl_3): δ 8.22 (d, $J = 16.2$ Hz, 1H), 8.03 (d, $J = 6.8$ Hz, 1H), 7.73 (d, $J = 15.3$ Hz, 2H), 7.63 (d, $J = 15.3$ Hz, 1H), 7.49 – 7.27 (m, 5H), 6.84 (t, $J = 6.6$ Hz, 1H), 6.12 (s, 2H), 3.90 (s, 6H), 3.86 (s, 3H); ^{13}C NMR (125 MHz, CDCl_3): δ 190.3, 163.1, 161.7, 145.6, 139.8, 134.9, 131.1, 128.3, 127.0, 126.9, 126.8, 126.4, 124.7, 123.2, 119.2, 119.1, 118.7, 118.6, 117.9, 113.1, 106.4, 90.4, 55.7, 55.4; HRMS (ESI): m/z calcd for $\text{C}_{27}\text{H}_{23}\text{F}_2\text{N}_2\text{O}_4$ 477.1620, found 477.1625 $[\text{M}+\text{H}]^+$.

4.2. Biological evaluation

4.2.0. Cell cultures

The cervical (HeLa), gastric (HGC-27), lung (NCI-H460), prostate (DU-145, PC-3) and breast (4T1) tumor cell lines were procured from National center for Cell science (NCCS), Pune, India. MTT [3-(4,5-dimethylthiazol-2-yl)-2,5-diphenyl tetrazolium bromide], trypsin-EDTA were bought from Sigma Chemicals Co (St. Louis, MO). DMEM, RPMI 1640 medium, fetal bovine serum were purchased from GIBCO-Invitrogen. The 12, 24 and 96 well flat bottom tissue culture plates were procured from Corning.

4.2.1. MTT assay

The anticancer activity of the compounds (**12a–t**) was determined by using MTT assay. $2.5\text{--}5 \times 10^3$ cells per well were seeded in 100 μL DMEM or RPMI, supplemented with 10% FBS in each well of 96-well microculture plates and incubated for 24 h at 37 °C in a CO_2 incubator. Compounds, diluted to the desired concentrations in culture medium, were added to the wells with respective vehicle control. After 48 h of incubation period, medium was discarded, 100 μL of MTT (3-(4,5-dimethylthiazol-2-yl)-2,5-diphenyl tetrazolium bromide) (0.5 mg/mL)

containing medium was added to each well and the plates were incubated for 4 h. The supernatant from each well was removed carefully, formazan crystals were dissolved in 200 μ L of DMSO and the absorbance was recorded at 570 nm wavelength with multimode plate reader (Spectramax M4, Molecular devices, USA).

4.2.2. Evaluation of tubulin polymerization inhibitory activity

Tubulin polymerization kit was procured from Cytoskeleton, Inc. (BK011). To assess the effect of compound **12t** on tubulin polymerization, a fluorescence based *in vitro* tubulin polymerization assay was carried out according to the manufacturer's protocol and Nocodazole was used as positive control. The reaction mixture having porcine brain tissue (2 mg/mL) in 80 mM PIPES at pH 6.9, 2.0 mM MgCl₂, 0.5 mM EGTA, 1.0 mM GTP and glycerol in the presence and absence of test compound (**12t**, at final concentration of 10 μ M) was prepared and added to each well of 96-well plate. Tubulin polymerization was followed by a time dependent increase in fluorescence due to the incorporation of a fluorescence reporter into microtubules as polymerization proceeds. Fluorescence emission at 440 nm (excitation wavelength is 360 nm) was measured using a Spectramax M4 Multi mode Micro plate Detection System. The IC₅₀ value was calculated from the compound concentration required to inhibit 50% of tubulin assembly in comparison to control.

4.2.3. Cell cycle analysis

To examine the effect of compound **12t** on cell cycle, cells were seeded in 12-well plates at a density of 1×10^5 cells/mL and allowed to attach for 24 h. Cells were treated with required concentrations (1 μ M and 2 μ M) of compound **12t** and incubated further for 24 h. The cells were collected, washed and fixed in 70% ethanol in PBS at -20 °C. After leaving overnight, the fixed cells were pelleted and stained with Propidium Iodide (25 μ g/mL) in the presence of RNase A (40 μ g/mL) containing 0.1% Triton X-100 for 0.5 h, at 37 °C in dark, and about 10000 events were analyzed using flow-cytometer (FACS verse, Becton Dickinson, US).

4.2.4. Acridine orange/ethidium bromide (AO/EB) staining

The morphological changes induced in PC-3 cells by compound **12t** were examined by Acridine Orange/Ethidium Bromide (AO/EB) staining. PC-3 cells were grown in 24 well plates (25000

cells/well) for 24 h and were treated with 0.5 μM , 1 μM and 2 μM concentration of compound **12t** for 48 h. After the incubation period, medium was discarded and cells were washed with PBS and treated with 10 $\mu\text{g}/\text{mL}$ of acridine orange and 10 $\mu\text{g}/\text{mL}$ of ethidium bromide. Morphological features were observed and photographs were taken immediately under fluorescence inverted microscope (Model: Nikon, Japan) using 488 nm excitation and 530 nm emission at 200x magnification.

4.2.5. Annexin V binding assay

PC-3 cells (1×10^5) were seeded in 12 well plates and allowed to grow overnight. Then, the medium was replaced with medium containing compound **12t** at 2 μM and 4 μM concentrations. After 24 h of treatment, cells from the supernatant and adherent monolayer cells were harvested by trypsinization, washed with PBS at 3000 rpm. Then the cells were processed using Annexin V-assay kit (FITC Annexin V Apoptosis Detection Kit, BD Pharmingen™) according to the manufacturer's protocol. Further, flow cytometric analysis was performed using a flow-cytometer (BD FACSVerse™, USA).

4.2.6. DAPI staining

PC-3 cells were seeded on 24 well plates at the density of 25000 cells/well and allowed to adhere overnight. Then, the cells were treated with 1 μM and 2 μM concentration of compound **12t** for 48 h, washed with PBS and fixed with 4% neutral buffered formalin solution for 20 min. Again, the cells were washed twice with PBS and permeabilized with 0.2% triton-x for 5 min and stained with DAPI (1 $\mu\text{g}/\text{mL}$) for 10 min at room temperature. Cells were examined for morphological changes under fluorescence microscope (Model: Nikon, Japan) using 350 nm excitation and 460 nm emission at 200x magnification.

4.2.7. Measurement of mitochondrial membrane potential (MMP)

Mitochondrial membrane potential (MMP) was determined using JC-1 dye as per method given by Atulya et al., with minor modifications [49]. PC-3 cells were cultured in 12 well plates at a density of 1×10^5 cells/mL and allowed to grow overnight. Then, the cells were treated with 2 μM and 4 μM of compound **12t** for 24 h. After treatment, cells were treated with JC-1 (2 μM)

dye and incubated for 45 min in dark at 37 °C in an incubator. Subsequently, cells were washed twice with PBS, trypsinized and analyzed by flow-cytometer (BD FACSVerse™, USA).

4.2.8. Measurement of reactive oxygen species (ROS) levels

PC-3 cells were seeded in 12 well plates at a density of 1×10^5 cells/mL and allowed to adhere for overnight. The cells were treated with 1 μ M and 2 μ M concentrations of compound **12t** for 24 h. The medium was replaced with culture medium containing DCFDA dye (10 μ M) and incubated for 0.5 h at room temperature in dark. The fluorescence intensity from each sample was analyzed at excitation wavelength of 488 nm and emission wavelength of 530 nm by flow-cytometer.

4.2.9. Computational methods

The 3D structure of compound **12t** was built on Maestro Molecule Builder of Schrödinger. The built molecule was optimized using OPLS_2005 force field in LigPrep module of Schrödinger software. Docking procedure was followed using the standard protocol implemented in Maestro, version 9.9 and the compound **12t** was docked against the colchicine binding site of α/β -tubulin interphase. The ligand –protein complex was analyzed for interactions and the 3D pose of most active compound **12t** was taken using Schrödinger and PyMOL v0.99.

4.2.10. Water solubility test

2 mg of curcumin/**12e/12t** was mixed with 2.0 mL of milli-Q water and the mixture was vortexed for 5 min, sonicated for 1 min, and incubated at 37 °C for 24 h. Then, the mixture was centrifuged at 14,000 rpm for 15 min and the water layer was separated and scanned in a spectrophotometer at a wavelength range of 200 – 600 nm.

Acknowledgements

Authors are thankful to DoP, Ministry of Chemicals & Fertilizers, Govt. of India, New Delhi, for the award of NIPER fellowship.

References

1. D.J. Newman, G.M. Cragg, K.M. Snader, Natural products as sources of new drugs over the

- period 1981-2002, *J. Nat. Prod.* 66 (2003) 1022–1037.
2. S. Shishodia, M.M. Chaturvedi, B.B. Aggarwal, Role of curcumin in cancer therapy, *Curr. Problems Cancer* 31 (2007) 243–305.
 3. Y.-Y. Xu, Y. Cao, H. Ma, H.-Q. Li, G.-Z. Ao, Design, synthesis and molecular docking of α,β -unsaturated cyclohexanone analogous of curcumin as potent EGFR inhibitors with antiproliferative activity, *Bioorganic Med. Chem.* 21 (2013) 388–394.
 4. S.-L. Lee, W.-J. Huang, W.W. Lin, S.-S. Lee, C.-H. Chen, Preparation and anti-inflammatory activities of diarylheptanoid and diarylheptylamine analogs, *Bioorganic Med. Chem.* 13 (2005) 6175–6181.
 5. C. Selvam, S.M. Jachak, R. Thilagavathi, A.K. Chakraborti, Design, synthesis, biological evaluation and molecular docking of curcumin analogues as antioxidant, cyclooxygenase inhibitory and anti-inflammatory agents, *Bioorganic Med. Chem. Lett.* 15 (2005) 1793–1797.
 6. J. Hong, M. Bose, J. Ju, J.H. Ryu, X. Chen, S. Sang, M.J. Lee, C.S. Yang, Modulation of arachidonic acid metabolism by curcumin and related beta-diketone derivatives: effects on cytosolic phospholipase A(2), cyclooxygenases and 5-lipoxygenase, *Carcinogenesis* 25 (2004) 1671–1679.
 7. D.K. Agrawal, P.K. Mishra, Curcumin and Its Analogues: Potential Anticancer Agents, *Med. Res. Rev.* 30 (2010) 818–860.
 8. G. Liang, S. Yang, H. Zhou, L. Shao, K. Huang, J. Xiao, Z. Huang, X. Li, Synthesis, crystal structure and anti-inflammatory properties of curcumin analogues, *Eur. J. Med. Chem.* 44 (2009) 915–919.
 9. G. Liang, X. Li, L. Chen, S. Yang, X. Wu, E. Studer, E. Gurley, P.B. Hylemon, F. Ye, Y. Li, H. Zhou, Synthesis and anti-inflammatory activities of mono-carbonyl analogues of curcumin, *Bioorganic Med. Chem. Lett.* 18 (2008) 1525–1529.
 10. S.K. Sandur, M.K. Pandey, B. Sung, K.S. Ahn, A. Murakami, G. Sethi, P. Limtrakul, V. Badmaev, B.B. Aggarwal, Curcumin, demethoxycurcumin, bisdemethoxycurcumin, tetrahydrocurcumin and turmerones differentially regulate anti-inflammatory and anti-proliferative responses through a ROS-independent mechanism, *Carcinogenesis* 28 (2007) 1765–1773.
 11. W.M. Weber, L.A. Hunsaker, C.N. Roybal, E.V. Bobrovnikova-Marjon, S.F. Abcouwer, R.E. Royer, L.M. Deck, D.L.V. Jagt, Activation of NF κ B is inhibited by curcumin and related

- enones, *Bioorganic Med. Chem.* 14 (2006) 2450–2461.
12. S. Gafner, S.-K. Lee, M. Cuendet, S. Barthelemy, L. Vergnes, S. Labidalle, R.G. Mehta, C.W. Boone, J.M. Pezzuto, Biologic evaluation of curcumin and structural derivatives in cancer chemoprevention model systems, *Phytochemistry* 65 (2004) 2849–2859.
 13. B.B. Aggarwal, A. Kumar, A.C. Bharti, Anticancer potential of curcumin: preclinical and clinical studies, *Anticancer Res.* 23 (2003) 363–398.
 14. O.P. Sharma, Antioxidant activity of curcumin and related compounds, *Biochem. Pharmacol.* 25 (1976) 1811–1812.
 15. A.J. Ruby, G. Kuttan, K.D. Babu, K.N. Rajasekharan, R. Kuttan, Anti-tumour and antioxidant activity of natural curcuminoids, *Cancer Lett.* 94 (1995) 79–83.
 16. J.L. Arbiser, N. Klauber, R. Rohan, R. van Leeuwen, M.T. Huang, C. Fisher, E. Flynn, H.R. Byers, Curcumin is an in vivo inhibitor of angiogenesis, *Mol. Med.* 4 (1998) 376–383.
 17. R.C. Srimal, B.N. Dhawan, Pharmacology of diferuloyl methane (curcumin), a non-steroidal anti-inflammatory agent, *J. Pharm. Pharmacol.* 25 (1973) 447–452.
 18. R. Srivastava, M. Dikshit, R.C. Srimal, B.N. Dhawan, Anti-thrombotic effect of curcumin, *Thromb. Res.* 40 (1985) 413–417.
 19. Y. Kiso, Y. Suzuki, N. Watanabe, Y. Oshima, H. Hikino, Antihepatotoxic principles of *Curcuma longa* rhizomes, *Planta Med.* 49 (1983) 185–187.
 20. P.S. Babu, K. Srinivasan, Hypolipidemic action of curcumin, the active principle of turmeric (*Curcuma longa*) in streptozotocin induced diabetic rats, *Mol. Cell. Biochem.* 152 (1995) 13–21.
 21. A. Goel, A.B. Kunnumakkara, B.B. Aggarwal, Curcumin as "Curecumin": from kitchen to clinic. *Biochem. Pharmacol.* 75 (2008) 787–809.
 22. K. Bairwa, J. Grover, M. Kania, S.M. Jachak, Recent developments in chemistry and biology of curcumin analogues, *RSC Adv.* 4 (2014) 13946–13978.
 23. P. Anand, A.B. Kunnumakkara, R.A. Newman, B.B. Aggarwal, Bioavailability of curcumin: problems and promises, *Mol. Pharm.* 4 (2007) 807–818.
 24. R.A. Sharma, H.R. McLelland, K.A. Hill, C.R. Ireson, S.A. Euden, M.M. Manson, M. Pirmohamed, L.J. Marnett, A.J. Gescher, W.P. Steward, Pharmacodynamic and pharmacokinetic study of oral *Curcuma* extract in patients with colorectal cancer, *Clin. Cancer Res.* 7 (2001) 1894–1900.

25. C.H. Hsu, A.L. Cheng, Clinical studies with curcumin, *Adv. Exp. Med. Biol.* 595 (2007) 471–480.
26. <http://www.clinicaltrial.gov/ct2/results?term¼curcumin>, accessed January 2014.
27. M.J. Rosemond, L. St John-Williams, T. Yamaguchi, T. Fujishita, J.S. Walsh, Enzymology of a carbonyl reduction clearance pathway for the HIV integrase inhibitor, S-1360: role of human liver cytosolic aldo-keto reductases, *Chem. Biol. Interact.* 147 (2004) 129–139.
28. Y.J. Wang, M.H. Pan, A.L. Cheng, L.I. Lin, Y.S. Ho, C.Y. Hsieh, J.K. Lin, Stability of curcumin in buffer solutions and characterization of its degradation products, *J. Pharm. Biomed. Anal.* 15 (1997) 1867–1876.
29. H. Luo, S. Yang, Y. Cai, Z. Peng, T. Liu, Synthesis and biological evaluation of novel 6-chloro-quinazolin derivatives as potential antitumor agents, *Eur. J. Med. Chem.* 84 (2014) 746–752.
30. R. Wang, C. Chen, X. Zhang, C. Zhang, Q. Zhong, G. Chen, Q. Zhang, S. Zheng, G. Wang, Q.-H. Chen, Structure–Activity Relationship and Pharmacokinetic Studies of 1,5-Diheteroaryl-penta-1,4-dien-3-ones: A Class of Promising Curcumin-Based Anticancer Agents, *J. Med. Chem.* 58 (2015) 4713–4726.
31. N. Samaan, Q. Zhong, J. Fernandez, G. Chen, A.M. Hussain, S. Zheng, G. Wang, Q.-H. Chen, Design, synthesis, and evaluation of novel heteroaromatic analogs of curcumin as anti-cancer agents, *Eur. J. Med. Chem.* 75 (2014) 123–131.
32. Q.-H. Chen, K. Yu, X. Zhang, G. Chen, A. Hoover, F. Leon, R. Wang, N. Subrahmanyam, E.A. Mekuria, L.H. Rakotondraibe, A new class of hybrid anticancer agents inspired by the synergistic effects of curcumin and genistein: Design, synthesis, and anti-proliferative evaluation, *Bioorganic Med. Chem. Lett.* 25 (2015) 4553–4556.
33. P.V.S. Ramya, S. Angapelly, L. Guntuku, C.S. Digwal, B.N. Babu, V.G.M. Naidu, A. Kamal, Synthesis and biological evaluation of curcumin inspired indole analogues as tubulin polymerization inhibitors, *Eur. J. Med. Chem.* 127 (2017) 100–114.
34. A.K. Bagdi, S. Santra, K. Monir, A. Hajra, Synthesis of imidazo [1,2-*a*] pyridines: a decade update, *Chem. Commun.* 51 (2015) 1555–1575.
35. L. Li, Z. Li, M. Liu, W. Shen, B. Wang, H. Guo, Y. Lu, Design, Synthesis and Antimycobacterial Activity of Novel Imidazo[1,2-*a*]pyridine Amide-Cinnamamide Hybrids, *Molecules* 21 (2016) 49–62.

36. A. Kamal, J.S. Reddy, M.J. Ramaiah, D. Dastagiri, E.V. Bharathi, M.V.P. Sagar, S.N.C.V.L. Pushpavalli, P. Ray, M. Pal-Bhadra, Design, synthesis and biological evaluation of imidazopyridine/pyrimidine-chalcone derivatives as potential anticancer agents, *Med. Chem. Commun.* 1 (2010) 355–360.
37. W. An, W. Wang, T. Yu, Y. Zhang, Z. Miao, T. Meng, J. Shen, Discovery of novel 2-phenyl-imidazo[1,2-*a*]pyridine analogues targeting tubulin polymerization as antiproliferative agents, *Eur. J. Med. Chem.* 112 (2016) 367–372.
38. M. Hayakawa, K.-i. Kawaguchi, H. Kaizawa, T. Koizumi, T. Ohishi, M. Yamano, M. Okada, M. Ohta, S.-i. Tsukamoto, F.I. Raynaud, P. Parker, P. Workman, M.D. Waterfield, Synthesis and biological evaluation of sulfonylhydrazonesubstituted imidazo[1,2-*a*]pyridines as novel PI3 kinase p110 α inhibitors, *Bioorganic Med. Chem.* 15 (2007) 5837–5844.
39. J.-B. Xi, Y.-F. Fang, B. Frett, M.-L. Zhu, T. Zhu, Y.-N. Kong, F.-J. Guan, Y. Zhao, X.-W. Zhang, H.-y. Li, M.-L. Ma, W. Hu, Structure-based design and synthesis of imidazo[1,2-*a*]pyridine derivatives as novel and potent Nek2 inhibitors with *in vitro* and *in vivo* antitumor activities, *Eur. J. Med. Chem.* 126 (2017) 1083–1106.
40. Y. Yang, Y. Zhang, L. Yang, L. Zhao, L. Si, H. Zhang, Q. Liu, J. Zhou, Discovery of imidazopyridine derivatives as novel c-Met kinase inhibitors: Synthesis, SAR study, and biological activity, *Bioorg. Chem.* 70 (2017) 126–132.
41. P.V.S. Ramya, S. Angapelly, A. Angeli, C.S. Digwal, M. Arifuddin, B.N. Babu, C.T. Supuran, A. Kamal, Discovery of curcumin inspired sulfonamide derivatives as a new class of carbonic anhydrase isoforms I, II, IX, and XII inhibitors, *J. Enzyme Inhib. Med. Chem.* 32 (2017) 1274–1281.
42. N. Qin, C.-B. Li, M.-N. Jin, L.-H. Shi, H.-Q. Duan, W.-Y. Niu, Synthesis and biological activity of novel tiliroside derivants, *Eur. J. Med. Chem.* 46 (2011) 5189–5195.
43. S. Feng, D. Hong, B. Wang, X. Zheng, K. Miao, L. Wang, H. Yun, L. Gao, S. Zhao, H.C. Shen, Discovery of Imidazopyridine Derivatives as Highly Potent Respiratory Syncytial Virus Fusion Inhibitors, *ACS Med. Chem. Lett.* 6 (2015) 359–362.
44. C. Enguehard-Gueiffier, C. Croix, M. Herve, J.-Y. Kazock, A. Gueiffier, M. Abarbri, Convenient Synthesis of Alkenyl-, Alkynyl-, and Allenyl-Substituted Imidazo[1,2-*a*]pyridines *via* Palladium-Catalyzed Cross-Coupling Reactions, *Helvetica Chimica Acta* 90 (2007) 2349–2367.

45. C. Enguehard, J.-L. Renou, V. Collot, M. Hervet, S. Rault, A. Gueiffier, Reactivity of 3-Iodoimidazo[1,2-*a*]pyridines Using a Suzuki-Type Cross-Coupling Reaction, *J. Org. Chem.* 65 (2000) 6572–6575.
46. T.J. Donohoe, J.A. Basutto, J.F. Bower, A. Rathi, Heteroaromatic Synthesis *via* Olefin Cross-Metathesis: Entry to Polysubstituted Pyridines, *Org. Lett.* 13 (2011) 1036–1039.
47. E. Rohrmann, R.G. Jones, H.A. Shonle, The Use of Chalcones in the Synthesis of Medicinal Intermediates, *J. Am. Chem. Soc.* 66 (1944) 1856–1857.
48. V. Naidu, U.M. Bandari, A.K. Giddam, K.R.D. Babu, J. Ding, K.S. Babu, B. Ramesh, R.R. Pragada, P. Gopalakrishnakone, Apoptogenic activity of ethyl acetate extract of leaves of *Memecylon edule* on human gastric carcinoma cells via mitochondrial dependent pathway, *Asian Pac. J. Trop. Med.* 6 (2013) 337–345.
49. A. Safavy, K.P. Raisch, S. Mantena, L.L. Sanford, S.W. Sham, N.R. Krishna, J.A. Bonner, Design and Development of Water-Soluble Curcumin Conjugates as Potential Anticancer Agents, *J. Med. Chem.* 50 (2007) 6284–6288.
50. C. Dyrager, M. Wickström, M. Fridén-Saxin, A. Friberg, K. Dahlén, E.A.A. Wallén, J. Gullbo, M. Grøtli, K. Luthman, Inhibitors and promoters of tubulin polymerization: Synthesis and biological evaluation of chalcones and related dienones as potential anticancer agents, *Bioorganic Med. Chem.* 19 (2011) 2659–2665.
51. K.T. Chan, F.Y. Meng, Q. Li, C.Y. Ho, T.S. Lam, Y. To, W.H. Lee, M. Li, K.H. Chu, M. Toh, Cucurbitacin B induces apoptosis and S phase cell cycle arrest in BEL-7402 human hepatocellular carcinoma cells and is effective via oral administration, *Cancer Lett.* 294 (2010) 118–124.
52. U.V. Mallavadhani, C.V. Prasad, S. Shrivastava, V. Naidu, Synthesis and anticancer activity of some novel 5,6-fused hybrids of juglone based 1,4-naphthoquinones, *Eur. J. Med. Chem.* 83 (2014) 84–91.
53. P. Sharma, T.S. Reddy, D. Thummuri, K.R. Senwar, N.P. Kumar, V.G.M. Naidu, S.K. Bhargava, N. Shankaraiah, Synthesis and biological evaluation of new benzimidazole-thiazolidinedione hybrids as potential cytotoxic and apoptosis inducing agents, *Eur. J. Med. Chem.* 124 (2016) 608–621.
54. S. Shrivastava, P. Kulkarni, D. Thummuri, M.K. Jeengar, V.G.M. Naidu, M. Alvala, G.B. Reddy, S. Ramakrishna, Piperlongumine, an alkaloid causes inhibition of PI3 K/Akt/ mTOR

- signaling axis to induce caspase-dependent apoptosis in human triple-negative breast cancer cells, *Apoptosis* 19 (2014) 1148–64.
55. D. Trachootham, J. Alexandre, P. Huang, Targeting cancer cells by ROS-mediated mechanisms: a radical therapeutic approach?, *Nat. Rev. Drug Discov.* 8 (2009) 579–591.
56. A. Nagarsenkar, L. Guntuku, S.D. Guggilapu, K.D. Bai, S. Gannaju, V.G.M. Naidu, N.B. Bathini, Synthesis and apoptosis inducing studies of triazole linked 3-benzylidene isatin derivatives, *Eur. J. Med. Chem.* 124 (2016) 782–793.
57. S. Marchi, C. Giorgi, J.M. Suski, C. Agnoletto, A. Bononi, M. Bonora, E. DeMarchi, S. Missiroli, S. Patergnani, F. Poletti, A. Rimessi, J. Duszynski, M.R. Wieckowski, P. Pinton, Mitochondria-Ros Crosstalk in the Control of Cell Death and Aging, *J. Signal Transduct.* 2012 (2012) 1–17.
58. R.B.G. Ravelli, B. Gigant, P.A. Curmi, I. Jourdain, S. Lachkar, A. Sobel, M. Knossow, Insight into tubulin regulation from a complex with colchicine and a stathmin-like domain, *Nature* 428 (2004) 198–202.
59. Schrödinger suite 2014-3; Schrödinger, LLC: New York, 2014.

Table, Figure and Scheme captions, Tables, Figures and Scheme

Table 1: *In vitro* anticancer activity (IC₅₀ in μM)^a of curcumin inspired imidazo[1,2-*a*]pyridine analogues (**12a–t**).

Table 2: Relative potency of curcumin inspired imidazo[1,2-*a*]pyridine analogues.

Figure 1. Structure of curcumin and its analogues.

Figure 2. Representative structures of some imidazo[1,2-*a*]pyridine drugs, drug candidates and imidazo[1,2-*a*]pyridine derivatives of biological interest.

Figure 3. Design of new curcumin inspired imidazo[1,2-*a*]pyridine analogues as anticancer agents.

Figure 4. SAR analysis of curcumin inspired imidazo[1,2-*a*]pyridine analogues.

Figure 5. UV-visible spectra of compounds **12e** and **12t**.

Figure 6. Effect of compound **12t** on tubulin polymerization.

Figure 7. Cell cycle analysis of PC-3 cells treated with (a) control, (b) compound **12t** at 1 μM and (c) 2 μM for 24 h using propidium iodide cell staining method. All assays were done in triplicate.

Figure 8. AO-EB staining of PC-3 cells treated with compound **12t**. (a) DMSO treated cells (control); (b, c and d) After 48 h of treatment with 0.5 μM , 1 μM and 2 μM of **12t** respectively.

Figure 9. Annexin V-FITC/propidium iodide dual staining assay. PC-3 cells were treated with compound **12t** and stained with Annexin V-FITC/PI and examined for apoptosis using flow-cytometer. The 10,000 cells from each sample were analyzed by flow cytometry. The percentage of cells positive for Annexin V-FITC and/or Propidium iodide is reported inside the quadrants. Cells in the lower left quadrant (Q1-LL: AV-/PI-): live cells; lower right quadrant (Q2-LR: AV+/PI-): early apoptotic cells; upper right quadrant (Q3-UR: AV+/PI+): late apoptotic cells and upper left quadrant (Q4-UL: AV-/PI+): dead cells.

Figure 10. Nuclear morphology of PC-3 cells stained with DAPI. PC-3 cells were treated with compound **12t** (at 1 μM and 2 μM) for 48 h and stained with DAPI. The images were captured with fluorescence microscope.

Figure 11. Effect of compound **12t** on mitochondrial membrane potential ($\Delta\Psi\text{m}$). PC-3 cells were treated with 2 μM and 4 μM of compound **12t** and stained with JC-1 and % populations of the cells with healthy mitochondria and cells with depolarized mitochondria in each sample were analyzed by flow cytometer (BD FACSVerse™, USA). Data were mean \pm SEM of three individual experiments. * $P < 0.05$ when compared to control (One way ANNOVA followed by Dunnet's multiple comparison test).

Figure 12. Effect of compound **12t** on intracellular Reactive Oxygen Species (ROS) levels. PC-3 cells were treated with compound **12t** (at 1 μM and 2 μM) and stained with DCFDA and cells were assessed using flow-cytometer. Data were mean \pm SEM of three individual experiments. * $P < 0.05$ ** $P < 0.01$ *** $P < 0.001$ vs. Ctrl when compared to control (One way ANNOVA followed by Dunnet's multiple comparison test).

Figure 13. a) Docking model of the most potent compound **12t** (magenta colour stick with solid surface) and b) its ligand-protein interactions in the colchicine binding site of α/β -tubulin interface (PDB ID: 1SA0). The red dashed lines represents hydrogen bonds.

Figure 14. Superimposition of co-crystallized ligand (green) and best docked pose of compound **12t** (magenta) in the colchicine binding site of α/β -tubulin interface (PDB ID: 1SA0).

Scheme 1: Synthesis of curcumin inspired imidazo[1,2-*a*]pyridine analogues **12a–t**; Reagents and conditions: (i) 15% NaOH, ethanol, 0 °C – rt, 2–3 h, 71–85%. (ii) Ethanol, reflux, 1 h, 74.3%; (iii) NIS, rt, 1 h, 65.1%; (iv) Pd(PPh₃)₄, Na₂CO₃, dioxane:H₂O = 8:2, 75 °C, 2–6 h, 65–73%; (v) LiAlH₄, THF, 0 °C – rt, 1 h, 67–71%; (vi) DMP, DCM, 0 °C, 1 h, 65–74%; (vii) CH₃ONa, ethanol, rt, 15 min, 63–82%.

Table 1: *In vitro* anticancer activity (IC₅₀ in μM)^a of curcumin inspired imidazo[1,2-*a*]pyridine analogues (**12a–t**).

Compound	HeLA ^b	HGC-27 ^c	NCI-H460 ^d	DU-145 ^e	PC-3 ^e	4T1 ^f	RWPE-1 ^g
12a	> 10	> 10	> 10	> 10	> 10	> 10	-
12b	> 10	> 10	> 10	> 10	> 10	> 10	-
12c	5.51 ± 0.10	7.08 ± 0.92	4.01 ± 0.20	3.38 ± 0.14	3.03 ± 0.02	3.38 ± 0.06	-
12d	> 10	> 10	> 10	> 10	> 10	> 10	-
12e	1.67 ± 0.34	5.38 ± 1.59	2.84 ± 0.08	3.71 ± 0.05	2.75 ± 0.35	1.68 ± 0.03	-
12f	> 10	> 10	> 10	> 10	> 10	> 10	-
12g	> 10	> 10	> 10	> 10	> 10	> 10	-
12h	> 10	> 10	> 10	> 10	> 10	> 10	-
12i	> 10	> 10	> 10	> 10	> 10	> 10	-
12j	> 10	> 10	> 10	> 10	> 10	> 10	-
12k	> 10	> 10	> 10	> 10	> 10	> 10	-
12l	> 10	> 10	> 10	> 10	> 10	> 10	-
12m	> 10	> 10	> 10	> 10	> 10	> 10	-
12n	6.66 ± 1.51	7.84 ± 1.55	4.28 ± 0.28	4.00 ± 0.29	3.64 ± 0.14	5.61 ± 0.13	-
12o	9.41 ± 0.6	8.77 ± 0.16	5.52 ± 0.41	5.63 ± 0.11	7.24 ± 0.37	4.69 ± 0.63	-
12p	> 10	> 10	> 10	> 10	> 10	> 10	-
12q	8.41 ± 0.31	10.27 ± 0.25	9.53 ± 0.17	8.46 ± 0.33	8.94 ± 1.18	9.72 ± 0.40	-
12r	4.93 ± 0.05	6.35 ± 0.02	3.11 ± 0.19	4.19 ± 0.14	2.84 ± 0.58	3.27 ± 0.07	-
12s	5.58 ± 0.15	3.38 ± 0.59	3.01 ± 0.11	4.87 ± 0.40	5.43 ± 0.35	3.45 ± 0.24	-
12t	2.53 ± 0.01	2.21 ± 0.25	2.63 ± 0.05	2.97 ± 0.08	2.11 ± 0.27	1.71 ± 0.11	4.23 ± 0.13
Curcumin	N. D.	N. D.	17.14 ± 0.72	33.12 ± 1.91	18.71 ± 1.06	N.D	-
Vincristine sulphate (nM)	N. D.	N. D.	N. D.	71.83 ± 6.01	28.11 ± 2.42	N. D.	-

^a 50% inhibitory concentration after 48 h of drug treatment and mean ± SD of three individual experiments performed in triplicate.

^b Human cervical cancer cell line.

^c Human gastric cancer cell line.

^d Human lung cancer cell line.

^e Human prostate cancer cell line.

^f Mouse breast cancer cell line.

^g Normal human prostate epithelial cells.

ND – Not determined.

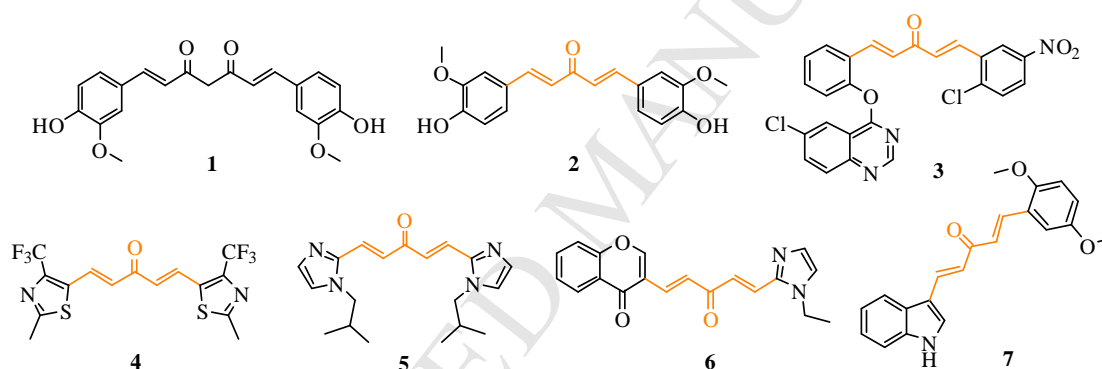
Table 2: Relative potency of curcumin inspired imidazo[1,2-*a*]pyridine analogues.

Compound	IC ₅₀ of curcumin/IC ₅₀ of compound ^a		
	NCI-H460 ^d	DU-145 ^e	PC-3 ^e
Curcumin	1	1	1
12c	4.3	9.8	6.1
12e	6.0	8.9	6.8
12n	4.0	8.3	5.1
12o	3.1	5.9	2.6
12q	1.8	3.9	2.1
12r	5.5	7.9	6.6
12s	5.7	6.8	3.4
12t	6.5	11.1	8.9

^aThe relative potency of curcumin mimics was calculated by dividing the IC₅₀ value of curcumin by that of each curcumin mimic.

^dHuman lung cancer cell line.

^eHuman prostate cancer cell line.

**Figure 1.** Structure of curcumin and its analogues.

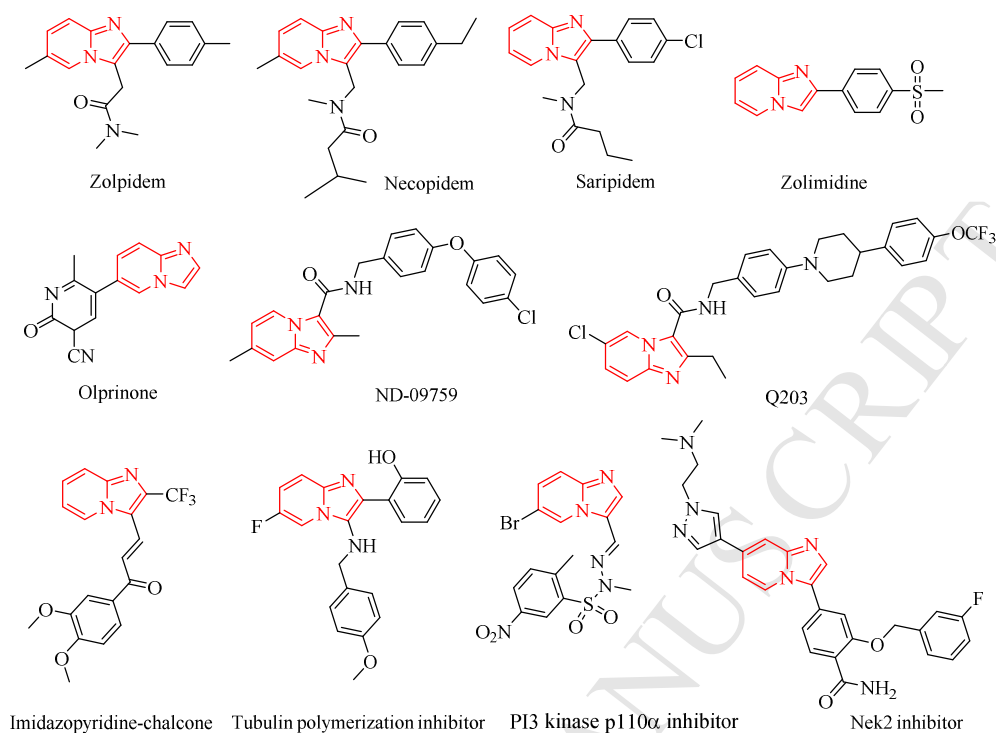


Figure 2. Representative structures of some imidazo[1,2-*a*]pyridine drugs, drug candidates and imidazo[1,2-*a*]pyridine derivatives of biological interest.

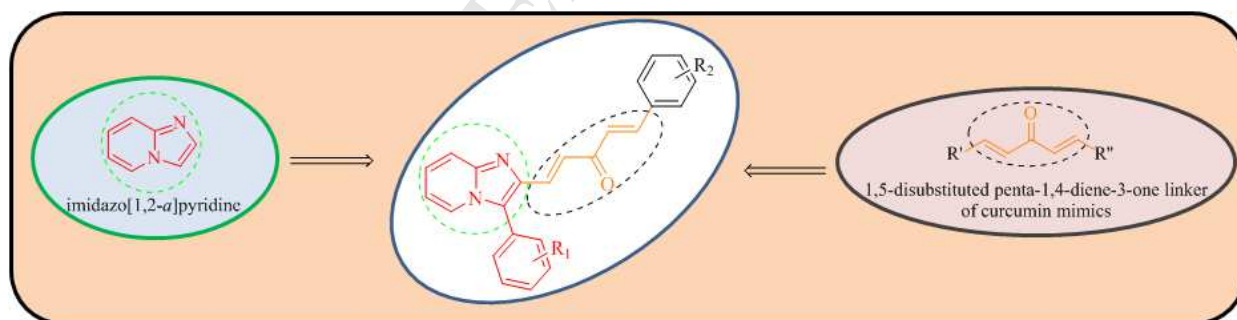


Figure 3. Design of new curcumin inspired imidazo[1,2-*a*]pyridine analogues as anticancer agents.

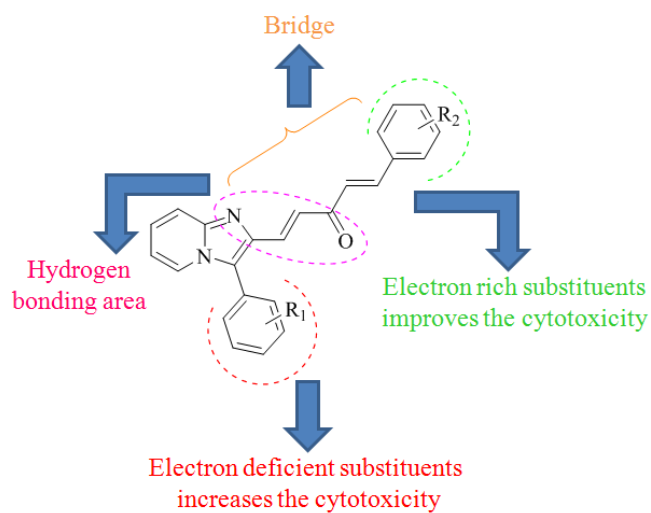


Figure 4. SAR analysis of curcumin inspired imidazo[1,2-*a*]pyridine analogues.

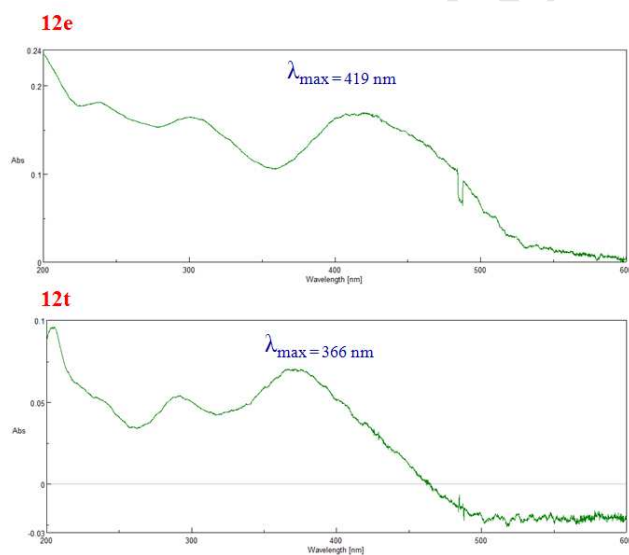


Figure 5. UV-visible spectra of compounds **12e** and **12t**.

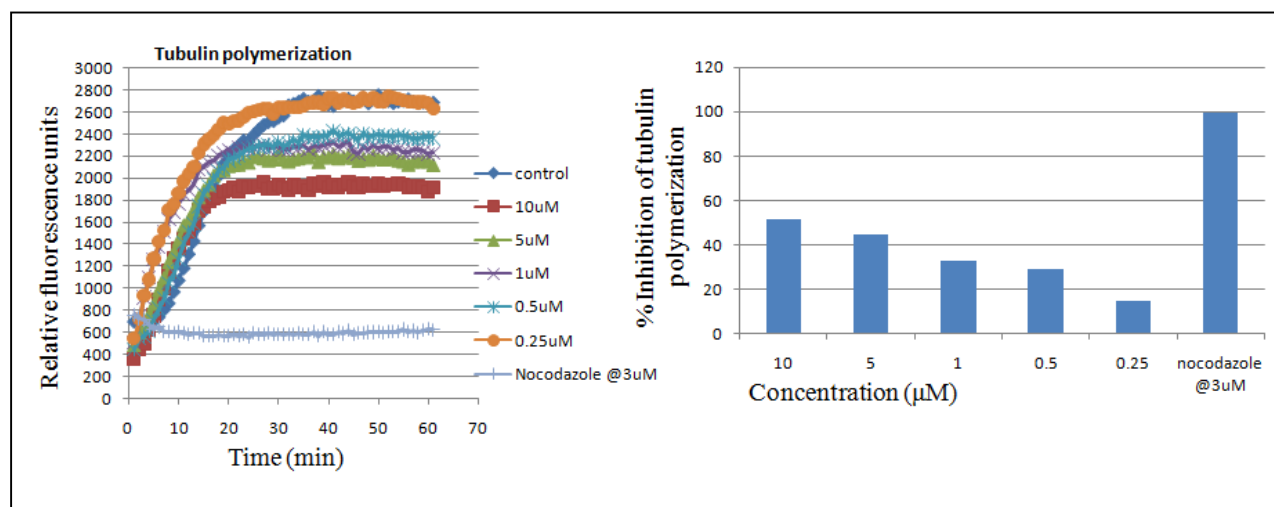


Figure 6. Effect of compound **12t** on tubulin polymerization.

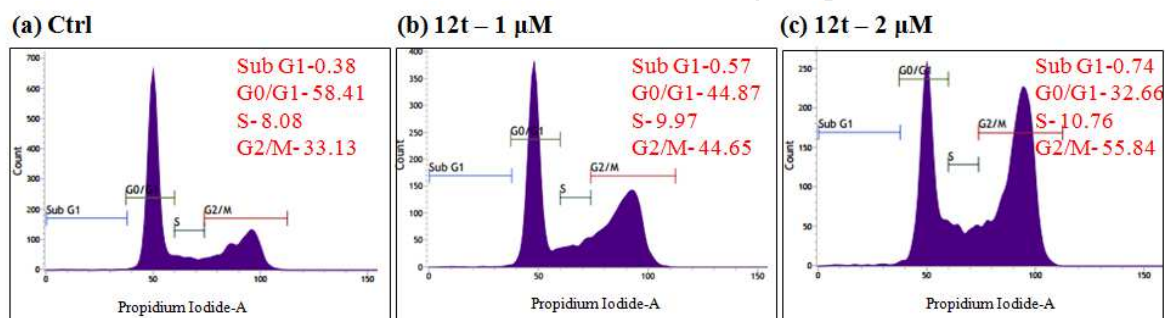


Figure 7. Cell cycle analysis of PC-3 cells treated with (a) control, (b) compound **12t** at 1 μM and (c) 2 μM for 24 h using propidium iodide cell staining method. All assays were done in triplicate.

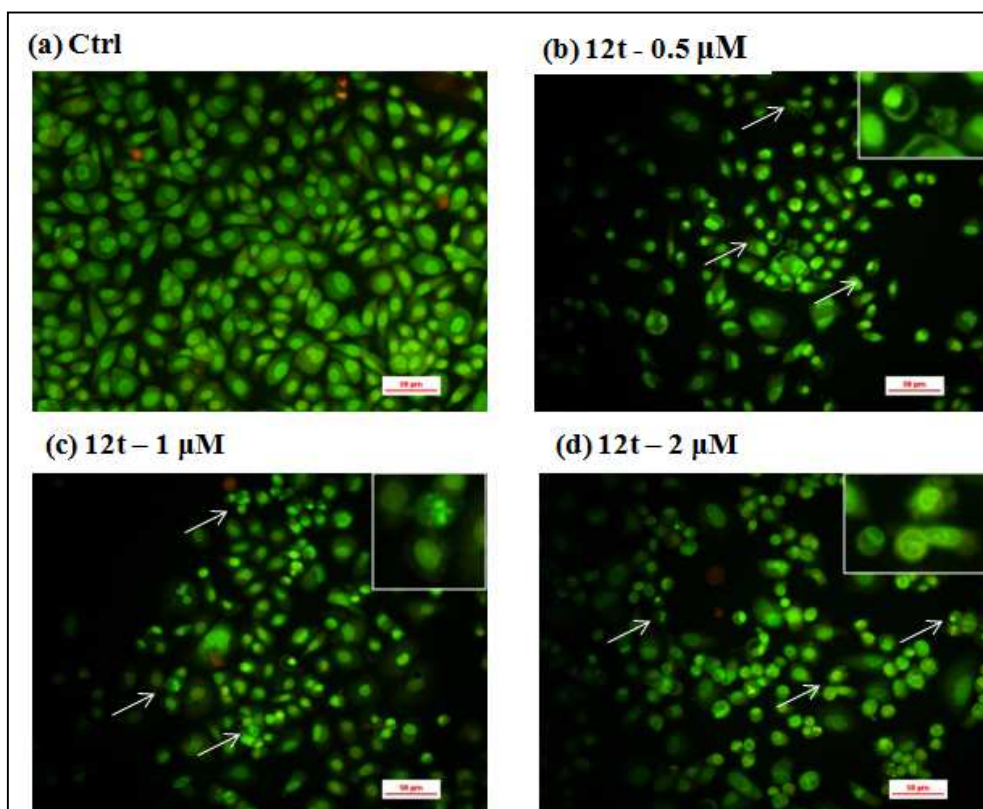


Figure 8. AO-EB staining of PC-3 cells treated with compound **12t**. (a) DMSO treated cells (control); (b, c and d) After 48 h of treatment with 0.5 μM , 1 μM and 2 μM of **12t** respectively.

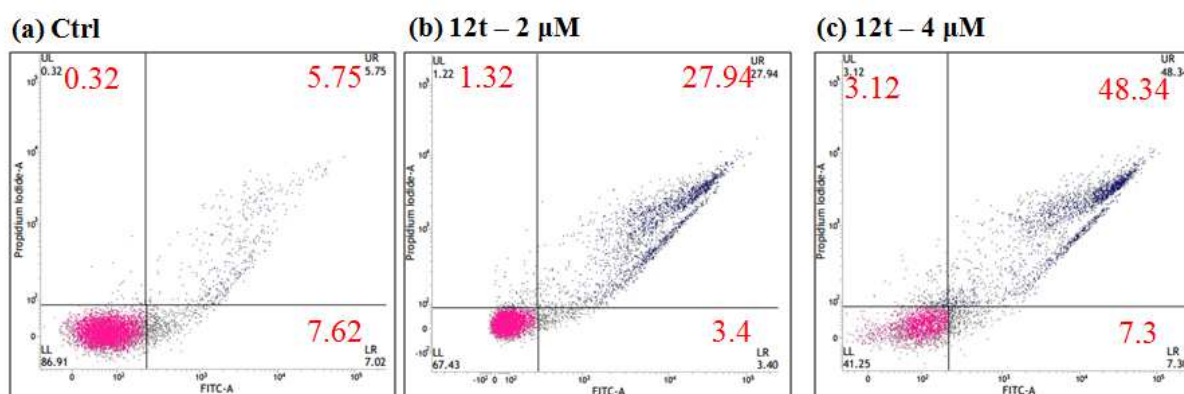


Figure 9. Annexin V-FITC/propidium iodide dual staining assay. PC-3 cells were treated with compound **12t** and stained with Annexin V-FITC/PI and examined for apoptosis using flow cytometer. The 10,000 cells from each sample were analyzed by flow cytometry. The percentage of cells positive for Annexin V-FITC and/or Propidium iodide is reported inside the quadrants. Cells in the lower left quadrant (Q1-LL: AV-/PI-): live cells; lower right quadrant (Q2-LR: AV+/PI-): early apoptotic cells; upper right quadrant (Q3-UR: AV+/PI+): late apoptotic cells and upper left quadrant (Q4-UL: AV-/PI+): dead cells.

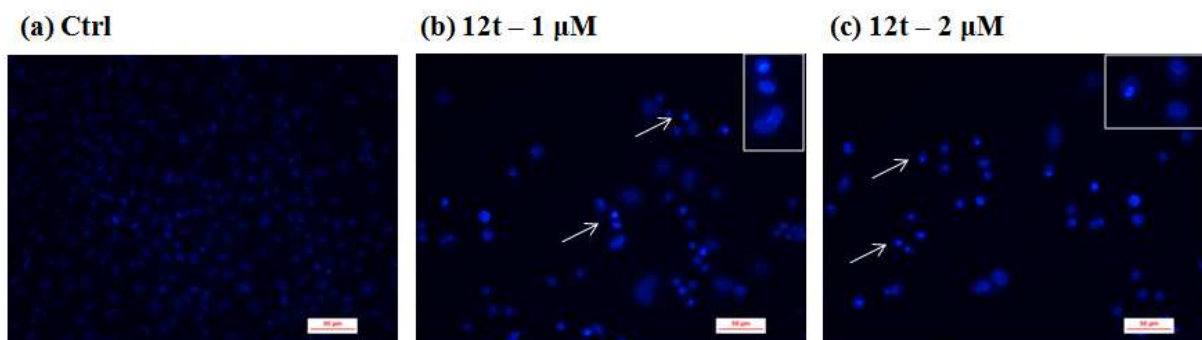


Figure 10. Nuclear morphology of PC-3 cells stained with DAPI. PC-3 cells were treated with compound **12t** (at 1 μM and 2 μM) for 48 h and stained with DAPI. The images were captured using fluorescence microscope.

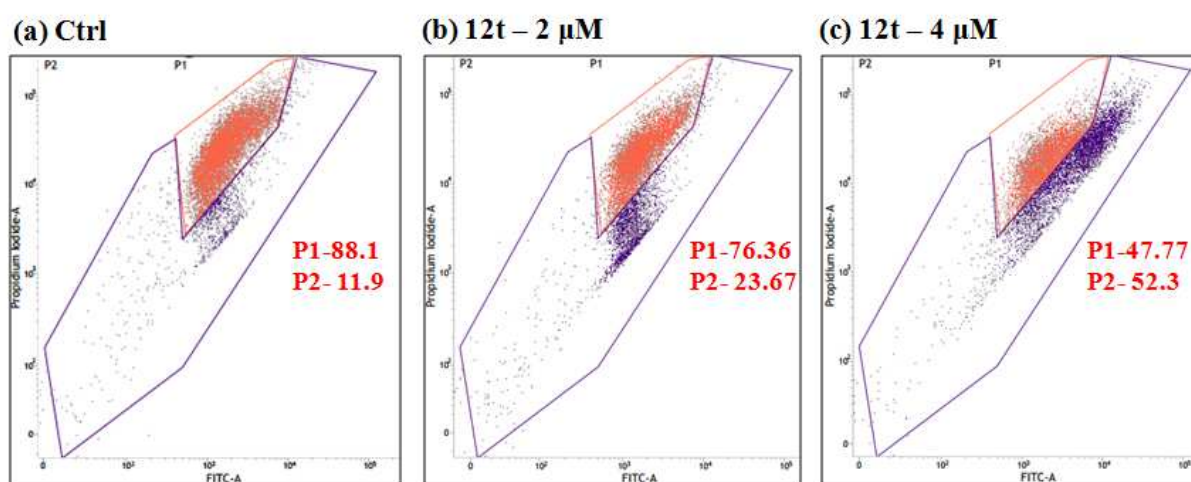


Figure 11. Effect of compound **12t** on mitochondrial membrane potential ($\Delta\Psi\text{m}$). PC-3 cells were treated with 2 μM and 4 μM of compound **12t** and stained with JC-1 and % populations of the cells with healthy mitochondria and cells with depolarized mitochondria in each sample were analyzed by flow cytometer (BD FACSVerse™, USA). Data were mean \pm SEM of three individual experiments. * $P < 0.05$ when compared to control (One way ANNOVA followed by Dunnet's multiple comparison test).

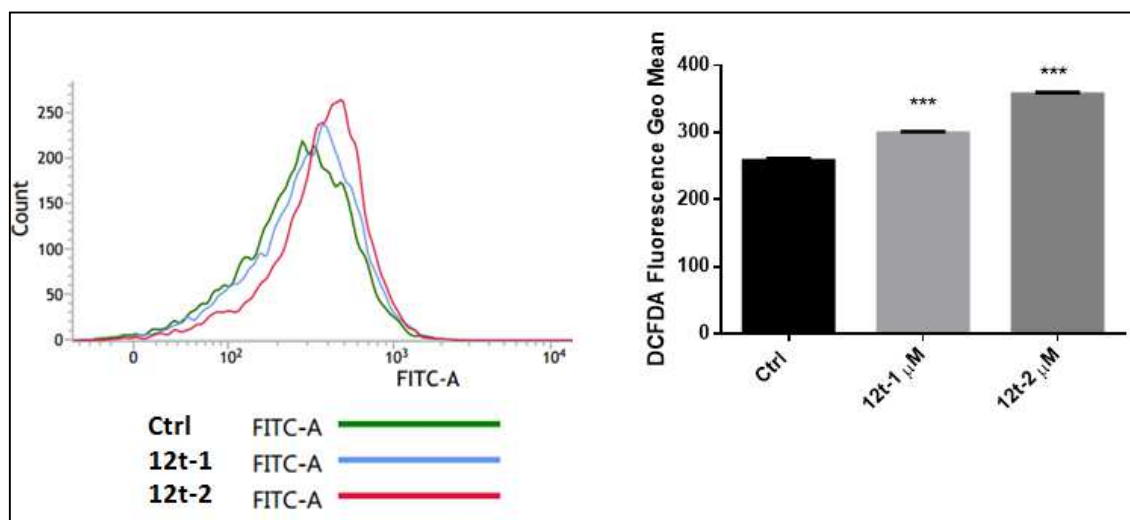


Figure 12. Effect of compound **12t** on intracellular Reactive Oxygen Species (ROS) levels. PC-3 cells were treated with compound **12t** (at 1 μM and 2 μM) and stained with DCFDA and cells were assessed using flow cytometer. Data were mean \pm SEM of three individual experiments. * $P < 0.05$ ** $P < 0.01$ *** $P < 0.001$ vs. Ctrl when compared to control (One way ANNOVA followed by Dunnet's multiple comparison test).

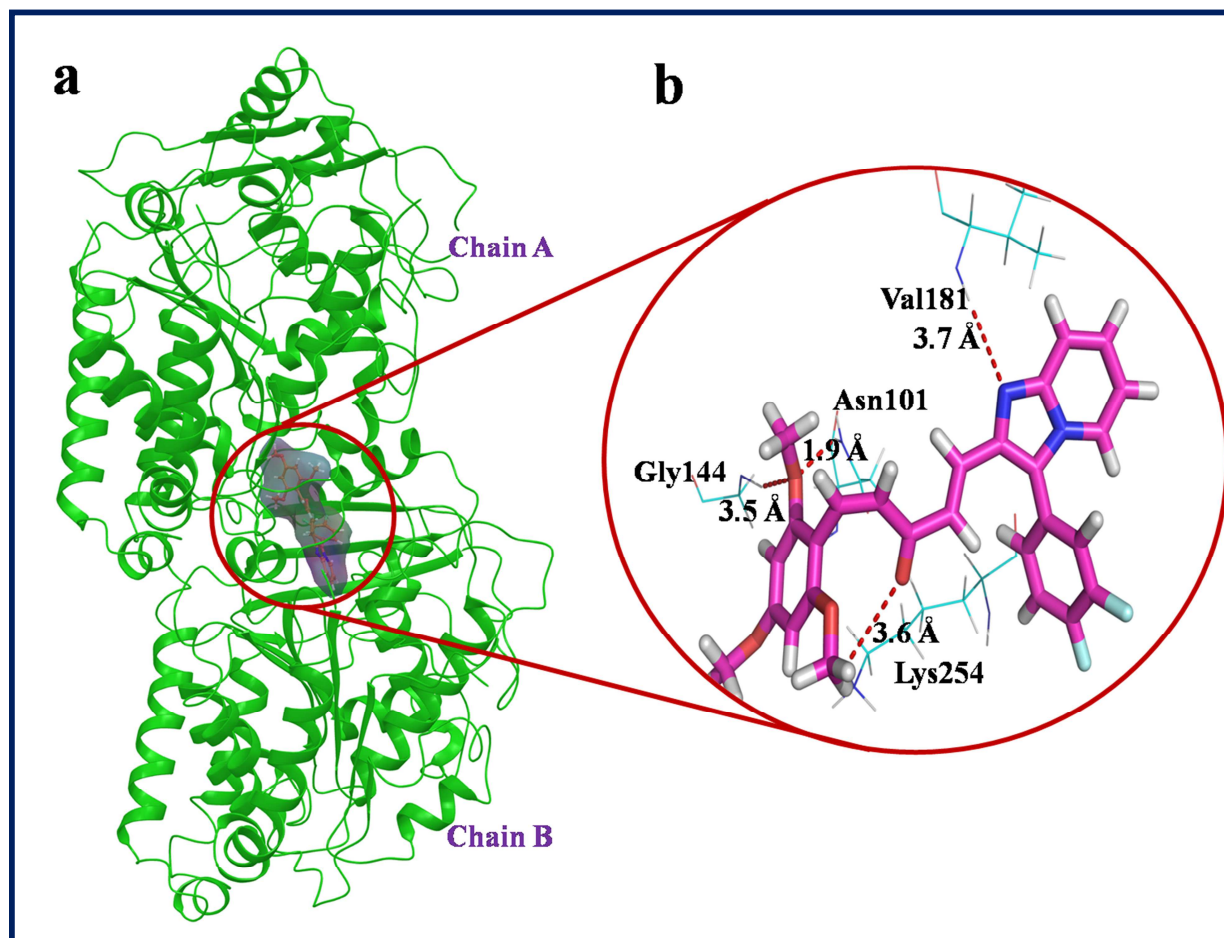


Figure 13. a) Docking model of the most potent compound **12t** (magenta colour stick with solid surface) and b) its ligand-protein interactions in the colchicine binding site of α/β -tubulin interface (PDB ID: 1SA0). The red dashed lines represents hydrogen bonds.

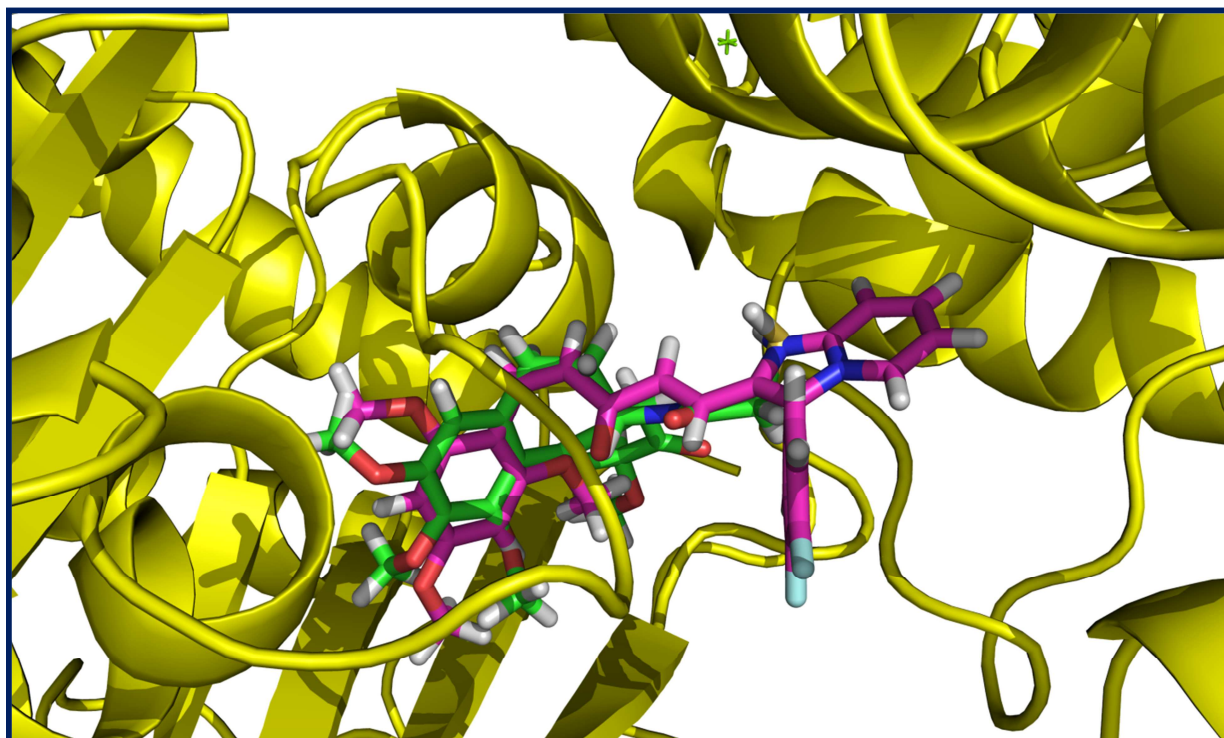
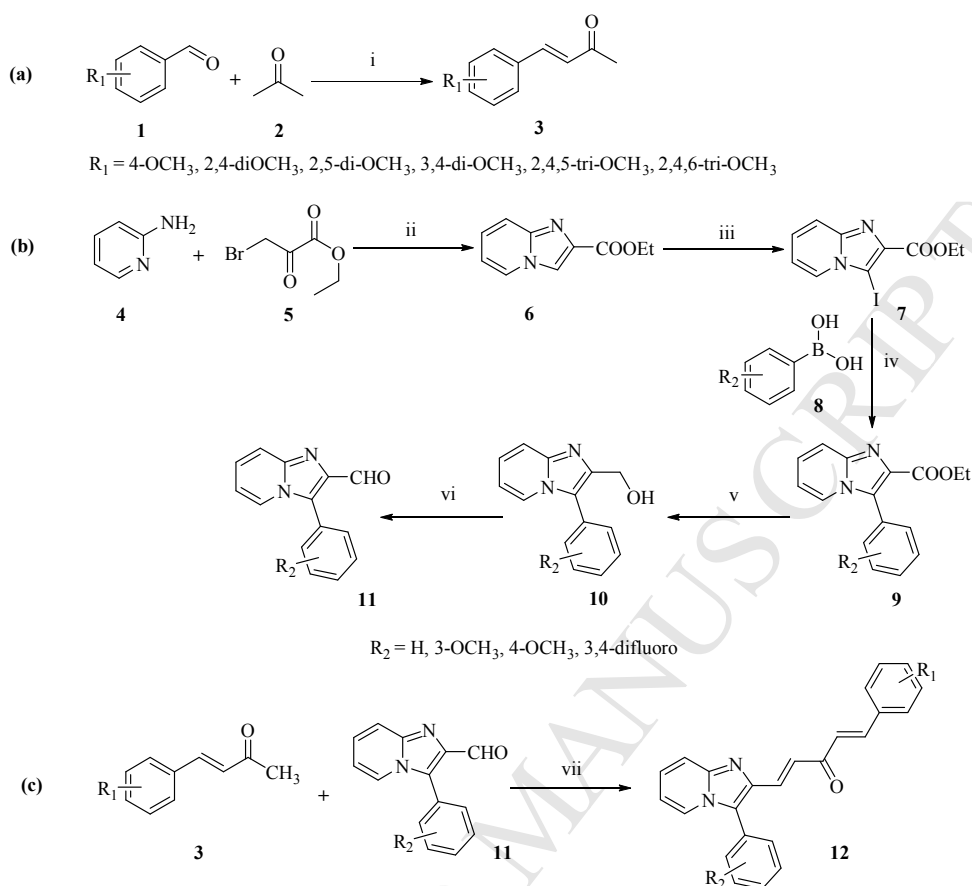


Figure 14. Superimposition of co-crystallized ligand (green) and best docked pose of compound **12t** (magenta) in the colchicine binding site of α/β -tubulin interface (PDB ID: 1SA0).



12a: $R_1 = \text{H}, R_2 = 4\text{-OCH}_3$

12b: $R_1 = \text{H}, R_2 = 2,4\text{-di-OCH}_3$

12c: $R_1 = \text{H}, R_2 = 2,5\text{-di-OCH}_3$

12d: $R_1 = \text{H}, R_2 = 3,4\text{-di-OCH}_3$

12e: $R_1 = \text{H}, R_2 = 2,4,5\text{-tri-OCH}_3$

12f: $R_1 = \text{H}, R_2 = 2,4,6\text{-tri-OCH}_3$

12g: $R_1 = 3\text{-OCH}_3, R_2 = 4\text{-OCH}_3$

12h: $R_1 = 3\text{-OCH}_3, R_2 = 2,4\text{-di-OCH}_3$

12i: $R_1 = 3\text{-OCH}_3, R_2 = 2,5\text{-di-OCH}_3$

12j: $R_1 = 3\text{-OCH}_3, R_2 = 3,4\text{-di-OCH}_3$

12k: $R_1 = 4\text{-OCH}_3, R_2 = 4\text{-OCH}_3$

12l: $R_1 = 4\text{-OCH}_3, R_2 = 2,4\text{-di-OCH}_3$

12m: $R_1 = 4\text{-OCH}_3, R_2 = 2,5\text{-di-OCH}_3$

12n: $R_1 = 4\text{-OCH}_3, R_2 = 3,4\text{-di-OCH}_3$

12o: $R_1 = 4\text{-OCH}_3, R_2 = 2,4,5\text{-tri-OCH}_3$

12p: $R_1 = 3,4\text{-difluoro}, R_2 = 4\text{-OCH}_3$

12q: $R_1 = 3,4\text{-difluoro}, R_2 = 2,4\text{-di-OCH}_3$

12r: $R_1 = 3,4\text{-difluoro}, R_2 = 2,5\text{-di-OCH}_3$

12s: $R_1 = 3,4\text{-difluoro}, R_2 = 3,4\text{-di-OCH}_3$

12t: $R_1 = 3,4\text{-difluoro}, R_2 = 2,4,6\text{-tri-OCH}_3$

Scheme 1: Synthesis of curcumin inspired imidazo[1,2-*a*]pyridine analogues **12a–t**; Reagents and conditions: (i) 15% NaOH, ethanol, 0 °C – rt, 2–3 h, 71–85%. (ii) Ethanol, reflux, 1 h, 74.3%; (iii) NIS, rt, 1 h, 65.1%; (iv) Pd(PPh₃)₄, Na₂CO₃, dioxane:H₂O = 8:2, 75 °C, 2–6 h, 65–73%; (v) LiAlH₄, THF, 0 °C – rt, 1 h, 67–71%; (vi) DMP, DCM, 0 °C, 1 h, 65–74%; (vii) CH₃ONa, ethanol, rt, 15 min, 63–82%.

Research Highlights

- New series of curcumin inspired imidazo[1,2-*a*]pyridine analogues were synthesized.
- Anticancer activity was tested on six cancer cell lines and one normal cell line.
- Compound **12t** effectively inhibited polymerization of tubulin in a cell-free assay.
- **12t** induced apoptosis and cell cycle arrest in G2/M phase in PC-3 cells.
- **12t** was almost 2 times more selective on PC-3 cells compared to RWPE-1 cells.